REPORT DOCUMENTATION PAGE

Form Approved OMB NO. 0704-0188

1. REPORT DATE (DD-MM-YYYY)	2. REPORT TYPE	3. DATES COVERED (From - To)
04-01-2011	Final Report	10-Jun-2009 - 9-Mar-2010

4. TITLE AND SUBTITLE
Electrochemically Promoted Organic Isomerization Reactions at Polymer Electrolyte Fuel Cell Cathodes

5a. CONTRACT NUMBER
W911NF-09-1-0289

5b. GRANT NUMBER

5c. PROGRAM ELEMENT NUMBER
622705

6. AUTHORS
Eugene Smotkin

5d. PROJECT NUMBER

5e. TASK NUMBER

5f. WORK UNIT NUMBER

7. PERFORMING ORGANIZATION NAMES AND ADDRESSES
Northeastern University
Office of Sponsored Programs
Northeastern University
Boston, MA 02115 -5000

8. PERFORMING ORGANIZATION REPORT NUMBER

9. SPONSORING/MONITORING AGENCY NAME(S) AND ADDRESS(ES)
U.S. Army Research Office
P.O. Box 12211
Research Triangle Park, NC 27709-2211

10. SPONSOR/MONITOR'S ACRONYM(S)
ARO

11. SPONSOR/MONITOR'S REPORT NUMBER(S)
56068-CH-II.1

12. DISTRIBUTION AVAILIBILITY STATEMENT
Approved for Public Release; Distribution Unlimited

13. SUPPLEMENTARY NOTES
The views, opinions and/or findings contained in this report are those of the author(s) and should not contrued as an official Department of the Army position, policy or decision, unless so designated by other documentation.

14. ABSTRACT
A significant cost of bench-top synthesis of small molecule target compounds is in the purchase and disposal of solvents for use in carrying out the reactions and purification of the raw product. The working electrode of a proton exchange membrane fuel cell provides a surface of tunable acidity capable of catalyzing certain reactions. This technique has the added advantage of not only providing a solvent-free environment for organic synthesis, but also increases the reaction kinetics. The progress of each reaction is monitored through the use of a fuel cell capable of

15. SUBJECT TERMS
Fuel Cell, Nafion, Organic Chemistry

16. SECURITY CLASSIFICATION OF:			17. LIMITATION OF ABSTRACT	15. NUMBER OF PAGES	19a. NAME OF RESPONSIBLE PERSON
a. REPORT	b. ABSTRACT	c. THIS PAGE			Eugene Smotkin
UU	UU	UU	UU		19b. TELEPHONE NUMBER: 617-373-7526

Report Title

Electrochemically Promoted Organic Isomerization Reactions at Polymer Electrolyte Fuel Cell Cathodes

ABSTRACT

A significant cost of bench-top synthesis of small molecule target compounds is in the purchase and disposal of solvents for use in carrying out the reactions and purification of the raw product. The working electrode of a proton exchange membrane fuel cell provides a surface of tunable acidity capable of catalyzing certain reactions. This technique has the added advantage of not only providing a solvent-free environment for organic synthesis, but also increases the reaction kinetics. The progress of each reaction is monitored through the use of a fuel cell capable of obtaining operando infrared spectra. This cell was also used in study of temperature dependent Stark tuning rates of adsorbed CO on a Pt electrode. The study demonstrated Nafion interaction with the Pt surface and through the use of polarization modulated infrared reflection adsorption spectroscopy (PM-IRRAS), attenuated total reflectance (ATR) spectroscopy, and density functional theory (DFT) the functional groups responsible for this interaction were identified and model for Nafion adsorption was derived and is in press in the Journal of the American Chemical Society.

List of papers submitted or published that acknowledge ARO support during this reporting period. List the papers, including journal references, in the following categories:

(a) Papers published in peer-reviewed journals (N/A for none)

Number of Papers published in peer-reviewed journals: 2.00

(b) Papers published in non-peer-reviewed journals or in conference proceedings (N/A for none)

Number of Papers published in non peer-reviewed journals: 0.00

(c) Presentations

Number of Presentations: 0.00

Non Peer-Reviewed Conference Proceeding publications (other than abstracts):

Number of Non Peer-Reviewed Conference Proceeding publications (other than abstracts): 0

Peer-Reviewed Conference Proceeding publications (other than abstracts):

Number of Peer-Reviewed Conference Proceeding publications (other than abstracts): 9

(d) Manuscripts

Number of Manuscripts: 1.00

Patents Submitted

Patents Awarded

Awards

Graduate Students

NAME	PERCENT_SUPPORTED
Ian Kendrick	1.00
FTE Equivalent:	**1.00**
Total Number:	**1**

Names of Post Doctorates

NAME	PERCENT_SUPPORTED
FTE Equivalent:	
Total Number:	

Names of Faculty Supported

NAME	PERCENT_SUPPORTED
FTE Equivalent:	
Total Number:	

Names of Under Graduate students supported

NAME	PERCENT_SUPPORTED
FTE Equivalent:	
Total Number:	

Student Metrics

This section only applies to graduating undergraduates supported by this agreement in this reporting period

The number of undergraduates funded by this agreement who graduated during this period:	0.00
The number of undergraduates funded by this agreement who graduated during this period with a degree in science, mathematics, engineering, or technology fields:.....	0.00
The number of undergraduates funded by your agreement who graduated during this period and will continue to pursue a graduate or Ph.D. degree in science, mathematics, engineering, or technology fields:.....	0.00
Number of graduating undergraduates who achieved a 3.5 GPA to 4.0 (4.0 max scale):	0.00
Number of graduating undergraduates funded by a DoD funded Center of Excellence grant for Education, Research and Engineering:	0.00
The number of undergraduates funded by your agreement who graduated during this period and intend to work for the Department of Defense	0.00
The number of undergraduates funded by your agreement who graduated during this period and will receive scholarships or fellowships for further studies in science, mathematics, engineering or technology fields:	0.00

Names of Personnel receiving masters degrees

NAME
Total Number:

Names of personnel receiving PHDs

NAME

Total Number:

Names of other research staff

NAME PERCENT_SUPPORTED

FTE Equivalent:

Total Number:

Sub Contractors (DD882)

Inventions (DD882)

Funds from the DURIP grant have led to the fabrication of two fuel cells capable of operando Fourier transformation infrared spectroscopy (FTIR) and X-ray absorption spectroscopy (XAS). The operando cell features an upper flow field with an aperture which allows for the installation and removal of a CaF_2 window for FTIR measurements and the cell to be used as an air breathing cell for XAS. The lower flow field is made of graphite as to not decrease the intensity of the x-ray beam. The cell is designed to interface with commercially available diffuse reflection accessories for FTIR systems. The second operando spectroscopy cell further optimizes the function of the cell by increasing the ease of which the cell is assembled while minimizing variables which would lead to inefficiencies in cell operation as well as an improved fuel delivery design. The operando spectroscopy cell was recently featured at the annual X-ray Absorption Fine Structure (XAFS) workshop at Brookhaven National Labs. This event marked the first time that measurements were taken from an operating fuel cell at the National Synchrotron Light Source (NSLS). The purpose of the experiment was to use XAFS to measure the amount of platinum oxides that formed at the cathode at various potentials.

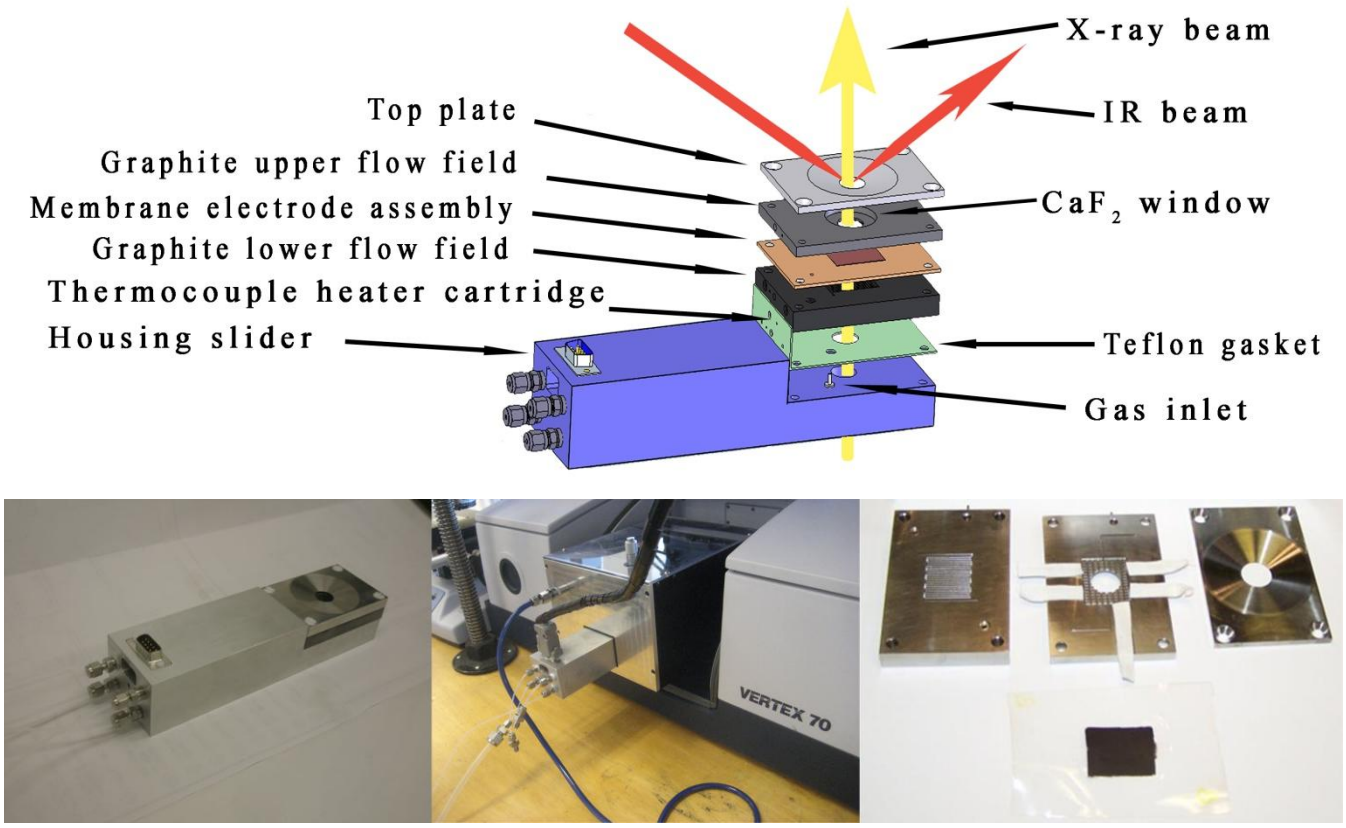

Figure 1: IR-XAS cell. Top: Red path, reflectance IR or fluorescence XAS; yellow path; transmission XAS. Bottom left: Assembled spectroscopy cell with DE9 connector for electrodes, heater cartridge and thermister. Bottom center: Cell installed in Pike diffuse reflectance accessory in a Bruker (Billerica, MA) Vertex 70 FTIR Spectrometer. Bottom right:

Bottom and top flow field with wicking material (white strips) adhered to upper flow field. MEA at bottom.

The spectroscopy cell was also used in an investigation of non-Faradaic electronic promotion of organic chemistry (EPOCH). EPOCH uses the superacidity of the proton exchange membrane (PEM) during fuel cell operation to provide a tunable surface to conduct electro-promoted organic reactions(*1-2*). So far these reactions have been limited to the isomerization and subsequent reduction of 1-butene. FTIR data collected from the spectroscopy cell shows an attenuation of the sp^2 C-H stretch indicative of 1-butene while and increased intensity in the sp^2 C-H peak corresponding with 2-butene.

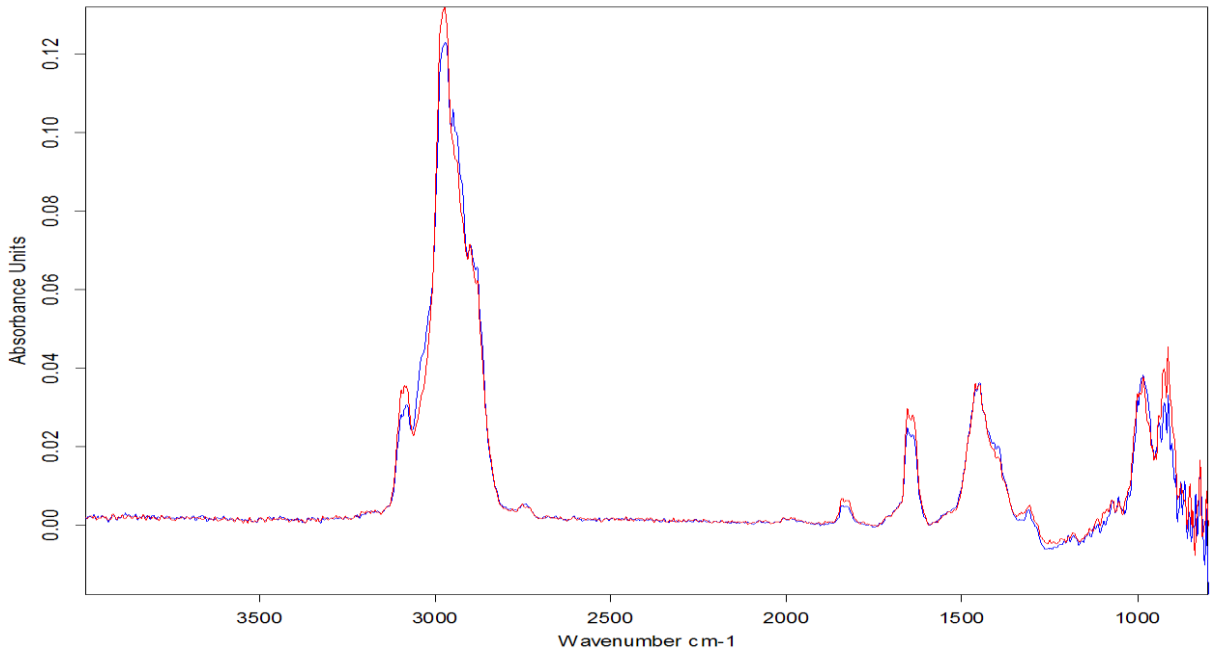

Figure 2: Infrared spectra of the isomerization of 1-butene through EPOCH. Red line corresponds with the spectrum of the reactant stream at OCV. Blue line corresponds with spectrum at 0V.

As it is a side product of methanol oxidation by platinum catalysis, the carbon monoxide poisoning of fuel cell catalysts is of interest to our research group. Previous infrared studies of carbon monoxide poisoning in direct methanol fuel cells has yielded Stark tuning data of carbon monoxide peaks absorbed onto counter electrodes(*3*). Stark tuning rates of absorbed carbon monoxide have also been studied on arc-melted Pt working electrodes in a three electrode cell(*4*). Using the spectroscopy cell previous discussed, research is being conducted into the Stark tuning rates of absorbed carbon monoxide on an operating fuel cell. The research will be looking at the effects, if any, of absorption potential on Stark tuning rates and the dependence of the temperature of the fuel cell on the infrared spectrum of absorbed Pt.

Funds have been used for the purchase of a Vertex 80 for use in an analysis of the infrared structure of Nafion-117. Attenuated total reflectance FTIR was used to determine the effect of cation substitution at the SO_3^- functionality on the overall spectrum. Bruker Opus 6.5 software processed the raw data and deconvoluted the peaks which allowed for proper correlation of

various functional groups in Nafion to specific peaks. An undergraduate within the group, using funds from this grant, developed a method using density functional theory (DFT)[5,6,7] calculations as well as the molecular modeling program Maestro, to predict the infrared stretches of the side chain of Nafion-112 to support peak assignments that have been previously made. The results of this project are currently being presented at the spring meeting of the Materials Research Society and have been published as communication to the editor in Macromolecules. Another graduate student is presenting data at the Materials Research Society meeting on the interaction between Nafion and Pt catalytic surface using polarization-modulated infrared-reflection absorption spectroscopy (PM-IRRAS). The PM-IRRAS technique allows for an enhanced characterization of the surface of Nafion. This graduate student and the PM-IRRAS setup were funded through the grant.

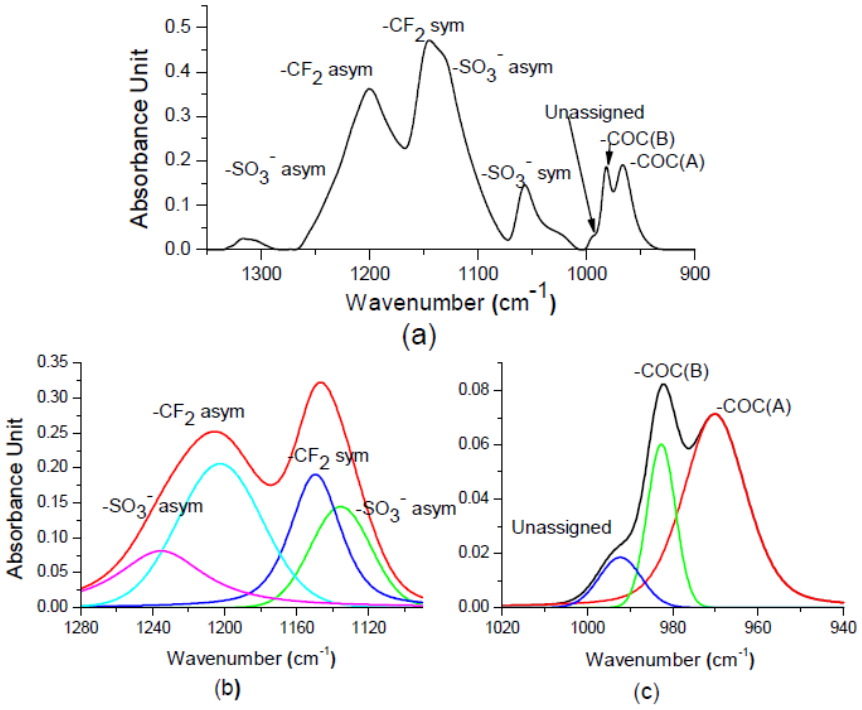

Figure 3: (a): ATR-FTIR of hydrated Nafion 117. (b) Deconvolution of 1100-1300 cm^{-1} region. (c) Deconvolution of 920-1020 cm^{-1} region.

The techniques described in this report, DFT, PM-IRRAS and operando spectroscopy have been used in concert to develop a new model of Nafion adsorption on Pt. Operando spectroscopy was used to study Stark tuning rates of carbon monoxide which demonstrated the adsorption of Nafion. PM-IRRAS was used to generate a spectra of the portions of Nafion interacting and with the Pt and a theoretical spectrum of Nafion was generated by DFT to identify the functionalities responsible for those interactions. The methodology developed in this research has applications beyond the study of Nafion and Pt and can be used in the study state-of-the-art solid electrolytes.

Presentations:

1. Kendrick, I. and Smotkin, E. S. Stark tuning of absorbed CO on fuel cell catalytic layers in operating fuel cells. In *Abstracts of Papers, 240th ACS National Meeting, Boston, MA, United States, August 22-26, 2010*. 2010.
2. Kumari, D.; Rivera, A.; Smotkin, E. S. Metal ion exchange method for assignment of IR peaks in ion exchange membranes. In *Abstracts of Papers, 239th ACS National Meeting, San Francisco, CA, United States, March 21-25, 2010*. 2010.
3. Kumari, D.; Smotkin, E.S.; Dimakis, N. DFT geometry optimization and vibrational frequencies of the quaternary ammonium cation-water [N (CH3)4 +OH-/ (H2O)n] clusters. In *Abstracts of Papers, 240th ACS National Meeting, Boston, MA, United States, August 22-26, 2010*. 2010.
4. Kumari, D.; Smotkin, E.S.; Grice, C. Durability studies on performance degradation of catalysts and Nafion membrane in direct methanol fuel cells. In *Abstracts of Papers, 240th ACS National Meeting, Boston, MA, United States, August 22-26, 2010*. 2010.
5. Webber, M., et al. Correlation of density functional theory calculations with transmission infrared spectroscopy of hydrated and dehydrated Nafion. In *Abstracts of Papers, 240th ACS National Meeting, Boston, MA, United States, August 22-26, 2010*. 2010.
6. Webber, M., et al. Correlation of XRD, SAXS and electro-active surface area analyses with catalyst performance. In *Abstracts of Papers, 240th ACS National Meeting, Boston, MA, United States,* August 22-26, 2010. 2010.
7. Webber, M.; Yakaboski, A.; Smotkin, E.S. DFT Modeling of Ionomer Exchange Group Solvation Water Structure. In *Polymer Materials and Membranes for Energy Devices,* Proceedings of the Materials Research Society, San Francisco, CA, April 5-9, 2010. 2010.
8. Yakaboski, A.P. and Smotkin, E. S. Influence of Nafion on adsorption of carbon monoxide on platinum catalysts. In *Abstracts of Papers, 240th ACS National Meeting, Boston, MA, United States, August 22-26, 2010*. 2010.
9. Yakaboski, A.; Webber, M.; Smotkin, E.S. PM-IRRAS: Nafion-Surface Interaction. In *Polymer Materials and Membranes for Energy Devices*, Proceedings of the Materials Research Society, San Francisco, CA, April 5-9, 2010. 2010.

Publications (reprints attached as appendix):

1. Kendrick, I.; Kumari, D.; Yakaboski, A.; Dimakis, N.; Smotkin, E.S. Elucidating the Ionomer-Electrode Interface. *J. Am. Chem. Soc.*, in press.
2. Kendrick, I.; Lewis, E.; Jia, Q.; Segre, C.; Smotkin, E.S. Operando X-Ray Adsorption Spectroscopy of Polymer Electrolyte Fuel Cells. *Anal. Chem.,* submitted for publication.
3. Webber, M., et al., *Mechanically Coupled Internal Coordinates of Ionomer Vibrational Modes.* Macromolecules, 2010. **43**(13): p. 5500-5502.

References:

1. Ploense, L., et al., *Proton spillover promoted isomerization of n-butylenes on Pd-black cathodes/Nafion 117.* Journal of the American Chemical Society, 1997. **119**(47): p. 11550-11551.

2. Ploense, L., et al., *Spectroscopic study of NEMCA promoted alkene isomerizations at PEM fuel cell Pd-Nafion cathodes.* Solid State Ionics, 2000. **136-137**: p. 713-720.
3. Bo, A.L., et al., *In situ Stark effects with inverted bipolar peaks for adsorbed CO on Pt electrodes in 50 degrees C direct methanol fuel cells.* Journal Of Physical Chemistry B, 2000. **104**(31): p. 7377-7381.
4. Liu, R., et al., *Potential-Dependent Infrared Absorption Spectroscopy of Adsorbed CO and x-ray Photoelectron Spectroscopy of Arc-Melted Single-Phase Pt, PtRu, PtOs, PtRuOs, and Ru Electrodes.* Journal of Physical Chemistry B, 2000. **104**(15): p. 3518-3531.

Appendix (reprints of manuscripts):

J|A|C|S
ARTICLES

Elucidating the Ionomer-Electrified Metal Interface

Ian Kendrick,[†] Dunesh Kumari,[†] Adam Yakaboski,[†] Nicholas Dimakis,[*,‡] and Eugene S. Smotkin[*,†]

Department of Chemistry and Chemical Biology, Northeastern University, 360 Huntington Avenue, Boston, Massachusetts 02115, United States, and Department of Physics and Geology, University of Texas—Pan American, 1201 West University Drive, Edinburg, Texas 78539, United States

Received September 9, 2010; E-mail: esmotkin@gmail.com; dimakis@utpa.edu

Abstract: The competitive adsorption of Nafion functional groups induce complex potential dependencies (Stark tuning) of vibrational modes of CO adsorbed (CO_{ads}) on the Pt of operating fuel cell electrodes. Operando infrared (IR) spectroscopy, polarization modulated IR spectroscopy (PM-IRRAS) of Pt—Nafion interfaces, and attenuated total reflectance IR spectroscopy of bulk Nafion were correlated by density functional theory (DFT) calculated spectra to elucidate Nafion functional group coadsorption responsible for the Stark tuning of CO_{ads} on high surface area fuel cell electrodes. The DFT calculations and observed spectra suggest that the side-chain CF_3, CF_2 groups (i.e., of the backbone and side chain) and the SO_3^- are ordered by the platinum surface. A model of the Nafion—Pt interface with appropriate dihedral and native bond angles, consistent with experimental and calculated spectra, suggest direct adsorption of the CF_3 and SO_3^- functional groups on Pt. Such adsorption partially orders the Nafion backbone and/or side-chain CF_2 groups relative to the Pt surface. The coadsorption of CF_3 is further supported by Mulliken partial charge calculations: The CF_3 fluorine atoms have the highest average charge among all types of Nafion fluorine atoms and are second only to the sulfonate oxygen atoms.

Introduction

The demand for renewable energy puts fuel cells at the forefront of energy conversion device development.[1−3] Polymer electrolyte membrane fuel cells (PEMFCs) incorporate an ionomer membrane (e.g., Nafion 117) for support of electrocatalytic layers and proton conduction between the electrodes and to maintain separation between the hydrogen and air.[4] A solubilized version of Nafion[5] (ionomer solution) is often used to prepare catalyst "inks" that are directly painted or decal transferred to the membrane.[6] The ionomer—metal interface formed after evaporation of the ink solvent is central to PEMFC electrocatalysis. For example, a spin coated Nafion layer on polycrystalline Pt enhances electrocatalysis.[7,8] Little is known about ionomer—metal interfaces. Markovic and co-workers probed Pt—electrolyte interfaces by measurements of CO oxidation currents, in sulfuric, perchloric, and KOH solutions, synchronized with IR absorption—reflection spectroscopy of linear (ν_{CO}^{l}) and bridge bound (ν_{CO}^{b}) CO_{ads} on Pt(111).[9] More recently their electrochemical studies on Pt(*hkl*)—Nafion interfaces suggest that the Nafion sulfonate group adsorbs onto the Pt surface.[10]

That the active state of a catalyst exists only during catalysis is rationale for operando (actual reactor conditions) characterization of the catalyst—ionomer interface.[11] A fuel cell membrane electrode assembly uniquely enables study of the ionomer metal interface without interferences due to mobile anions characteristic of aqueous acidic electrolytes. Operando fuel cell infrared (IR) spectroscopy was introduced by Fan et al.[12] In this report the aggregate of operando spectroscopy of fuel cell membrane electrode surfaces, attenuated total reflectance spectroscopy of Nafion 117, polarization modulated IR reflection absorption spectroscopy of Nafion spin-coated onto Pt, and density functional theory calculated Nafion spectra suggest a model for the Pt—Nafion interface that includes the Nafion CF_3 group as an important coadsorbate at the ionomer—Pt interface.

Experimental Section

Attenuated Total Reflectance (ATR) Spectroscopy. A surface pressure of 815 psi was maintained over the 1.8 mm diameter ATR crystal. Spectra were obtained using a Bruker Vertex 70 and Vertex 80 V vacuum FTIR spectrometer (Bruker, Billerica, MA). A MIRacle ATR accessory (Pike Technologies Spectroscopic Creativ-

[†] Northeastern University.
[‡] University of Texas-Pan American.

(1) Demirdoven, N.; Deutch, J. *Science* **2004**, *305*, 974.
(2) Diat, O.; Gebel, G. *Nat. Mater.* **2008**, *7*, 13.
(3) Hoogers, G., Ed.; *Fuel Cell Systems Explained*, 2nd ed.; CRC Press LLC: Boca Raton, FL, 2003.
(4) Gottesfeld, S.; Zawodzinski, T. A. *Advances in Electrochemical Science and Engineering*; Wiley-VCH: 1997; Vol. 5.
(5) Martin, C. R.; Rhoades, T. A.; Ferguson, J. A. *Anal. Chem.* **1982**, *54*, 1639.
(6) Wilson, M. S.; Gottesfeld, S. *J. Appl. Electrochem.* **1992**, *22*, 1.
(7) Liu, L.; Viswanathan, R.; Liu, R. X.; Smotkin, E. S. *Electrochem. Solid State Lett.* **1998**, *1*, 123.
(8) Ploense, L.; Salazar, M.; Gurau, B.; Smotkin, E. S. *Solid State Ionics* **2000**, *136—137*, 713.
(9) Stamenkovic, V.; Chou, K. C.; Somorjai, G. A.; Ross, P. N.; Markovic, N. M. *J. Phys. Chem. B* **2005**, *109*, 678.
(10) Subbaraman, R.; Strmcnik, D.; Stamenkovic, V.; Markovic, N. M. *J. Phys. Chem. C* **2010**, *114*, 8414.
(11) Topsoe, H. *J. Catal.* **2003**, *216*, 155.
(12) Fan, Q.; Pu, C.; Lay, K. L.; Smotkin, E. S. *J. Electrochem. Soc.* **1996**, *143*, L21.

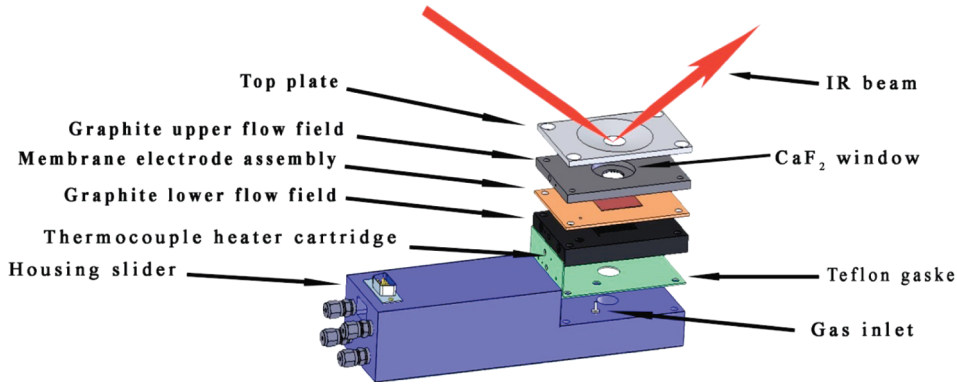

Figure 1. Exploded view schematic of operando spectroscopy cell.

ity, Madison, WI) with a ZnSe ATR crystal was used. The spectra were signal averaged from 100 scans at 4 cm^{-1} resolution with a dry-air purge at ambient temperature. Atmospheric compensation (to eliminate H_2O and CO_2 interference in the beam path) was used in all measurements. Data processing for all infrared data was done with the Bruker OPUS 6.5 software.

Preparation of Arc-Melt Pt. The preparative method for arc-melted electrodes has been described.[13] Briefly, the arc-melter (Materials Research Furnaces, Sun Cook, NH) was charged with 3 mm Pt shot (99.9+%, Sigma-Aldrich, St. Louis, MO). The chamber was evacuated to −29 psig and purged with argon three times. The Pt was arc-melted at 75 A under an Ar bleed. The chamber was vented to flip and arc-melt the sample three times. The Pt slug was epoxied (Devcon HP250, Danvers, MA) to a modified glass syringe barrel, cut flat using a diamond cutoff saw (Buehler IsoMet 1000, Lake Bluff, IL), and finally polished to a mirror finish using 0.05 μm aluminum oxide (Magner Scientific, Dexter, MI). The electrode was sonicated in Nanopure water (Milli-Q, Billerica, MA) for 10 min. Nafion ionomer solution (20 μL) was pipetted onto the Pt electrode assembly mounted on an inverted electrode rotator (Pine Instrument Company, Grove City, Pa) and then rotated (1000 rpm, 1 min).

Polarization Modulated Infrared Reflection Absorption Spectra (PM-IRRAS). The Vertex 80 V spectrometer was equipped with a Hinds II/ZS50 photoelastic modulator (Hinds Instruments, Hillsboro, OR), SR830 lock-in amplifier (Stanford Research Systems, Sunnyvale, CA), and a D3131\6 MCT detector (Infrared Associates, Stuart, FL). The angle of incidence was 60°, and the photoelastic modulator frequency was 50.14 kHz. The PM-IRRAS cell design has been reported.[14,15] Spectra were averaged (710 scans; 4 cm^{-1} resolution). Li-exchanged Nafion was prepared by soaking Nafion samples in 0.1 M salt solutions.

Computational Method. Unrestricted DFT[16,17] with the X3LYP[18] functional was used for geometry optimization and calculations of the normal-mode frequencies and corresponding IR spectra of the deprotonated and protonated Nafion side-chain and backbone segment. The backbone-segment terminal ends were substituted with CH_3 groups to eliminate computational interference with the Nafion CF_3 group. Jaguar 6.5 (Schrodinger Inc., Portland, OR) was used with the all-electron 6-311G**++ Pople triple-ζ basis set ("**" and "++" denote polarization[19] and diffuse[20] basis set functions, respectively). Output files were converted to vibrational mode animations using Maestro (Schrodinger Inc.). Calculations were carried out on a 55 node (dual core Xeon processors with 4GB RAM) High Performance Computing Cluster at the University of Texas, Pan American.

Membrane Electrode Assembly Preparation. Nafion-117 (E. I. DuPont) was immersed in boiling ~8 M nitric acid for 20 min, rinsed with Nanopure water, and finally immersed in boiling water for 1 h. Catalyst inks were prepared as previously described.[21,22] Briefly, Pt black (Johnson Matthey) was dispersed in a 5 wt % Nafion ionomer solution (Sigma Aldrich, Milwaukee, WI) diluted with Nanopure water and isopropyl alcohol. Inks were applied directly to a 5 cm^2 area of Nafion immobilized on a temperature controlled vacuum table (NuVant Systems Inc., Crown Point, IN) at 70 °C. The catalyst loadings were 4 mg/cm^2 of Pt black. The carbon paper gas diffusion layers (Toray Industries, Tokyo, Japan) were blocked with Vulcan XC-72 (Cabot Corporation, Billerica, MA).

Operando Spectroscopy. Temperature dependent CO_{ads} Stark tuning data were acquired by operando specular reflectance IR spectroscopy using a cell (Figure 1) based on the design of Fan et al.[12] The cell, controlled by an EZstat potentiostat (NuVant Systems Inc.), interfaces to a diffuse reflectance accessory (Pike Technologies, Madison, WI) installed on the Vertex 70 spectrometer. The IR beam accesses the working electrode surface through a CaF_2 window inserted into the upper flow field and a small slot in the carbon gas diffusion layer. The lower flow field electrode serves as both a hydrogen reference and counter electrode when charged with hydrogen. The small CO oxidation currents do not measurably polarize the hydrogen counter electrode. The working electrode was cycled (50 times) from 0 to1.2 V vs the hydrogen counter electrode. Spectra were obtained by averaging 250 scans at 4 cm^{-1} resolution. The cell was brought to the desired temperature and potential (300 mV) for the acquisition of reference spectra. Carbon monoxide was passed over the working electrode for 15 min. The cell was purged with N_2 (15 min) prior to setting the potential to 100 mV. Replicates of four spectra were acquired at 50 mV increments until the CO vibrational bands were no longer observable.

Results and Discussion

Operando Spectroscopy. Stark tuning plots of CO_{ads} on Pt in a fuel cell operated at 30, 50, and 70 °C (Figure 2) show a remarkable similarity to plots obtained by Stamenkovic et al. in sulfuric acid.[9] They correlated complex potential dependences (Stark tuning), of CO_{ads} vibrational frequencies (i.e., $d\nu_{CO}^{l}/dE$

(13) Ley, K. L.; Liu, R.; Pu, C.; Fan, Q.; Leyarovska, N.; Segre, C.; Smotkin, E. S. *J. Electrochem. Soc.* **1997**, *144*, 1543.
(14) Kunimatsu, K.; Golden, W. G.; Seki, H.; Philpott, M. R. *Langmuir* **1985**, *1*, 245.
(15) Kunimatsu, K. *J. Electroanal. Chem.* **1986**, *213*, 149.
(16) Hohenberg, P.; Kohn, W. *Phys. Rev. B* **1964**, *136*, B864.
(17) Kohn, W.; Sham, L. J. *Phys. Rev.* **1965**, *140*, 1133.
(18) Xu, X.; Zhang, Q.; Muller, R. P.; Goddard, W. A. *J. Chem. Phys.* **2005**, *122*, 14.
(19) Frisch, M. J.; Pople, J. A.; Binkley, J. S. *J. Chem. Phys.* **1984**, *80*, 3265.
(20) Clark, T.; Chandrasekhar, J.; Spitznagel, G. W.; Schleyer, P. *J. Comput. Chem.* **1983**, *4*, 294.
(21) Gurau, B.; Smotkin, E. *J. Power Sources* **2002**, *112*, 339.
(22) Stoupin, S.; Chung, E.-H.; Chattopadhyay, S.; Segre, C. U.; Smotkin, E. S. *J. Phys. Chem. B* **2006**, *110*, 9932.

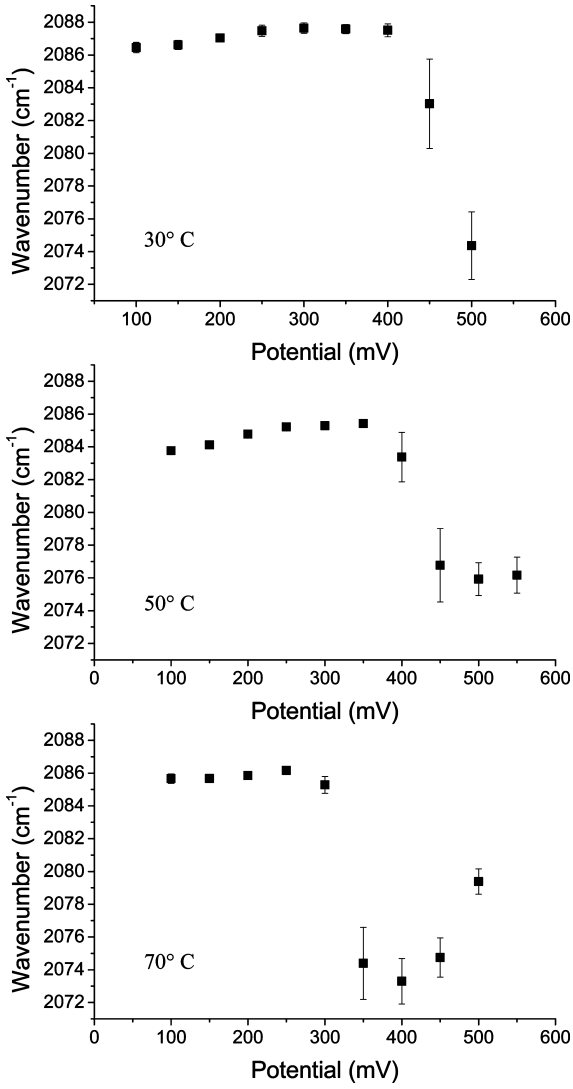

Figure 2. Stark tuning of adsorbed CO on the Pt membrane electrode assembly of an operating fuel cell.

and $d\nu_{CO}^{b}/dE$) in 0.5 M H_2SO_4, to the compression/dissipation of CO_{ads} islands: after a linear region from 0.1 to 0.3 V ($d\nu_{CO}^{l}/dE = 31$ cm^{-1}/V), a subtle ν_{CO}^{l} blue shift from the extrapolated linear region was followed by a precipitous drop, initiating at 0.5 V, that finally upturns at 0.65 V. They attribute this behavior to CO_{ads} island compression due to repulsive dipole interactions with a coadsorbed bisulfate ion initially observable at 0.35 V. CO_{ads} oxidation initiating at 0.5 V, induced by OH^- absorption, diminishes dipole−dipole coupling[23] and thus decreases $d\nu_{CO}^{l}/dE$. The upturn is attributed to an increased absorption of HSO_3^- relative to OH^-, which reestablishes repulsive dipole interactions that compress CO_{ads} islands and increase ν_{CO}^{l}. The plots in Figure 2 demonstrate an adsorption phenomenon onto Pt despite the lack of mobile ions typical of dilute sulfuric acid solutions. The fuel cell operando spectroscopy suggests a need for elucidation of Nafion functional groups responsible for modulation of CO/Pt interactions (i.e., Stark tuning).

Figure 3 shows the linear temperature dependence of the frequency at which the Stark tuning curves precipitously decrease: higher operating temperatures lower the potential at which CO oxidizes (−2.88 cm^{-1}/K, $R^2 = 0.991$). The relationship of this linear variation to the kinetics of the inner sphere processes[24] will be addressed in future work.

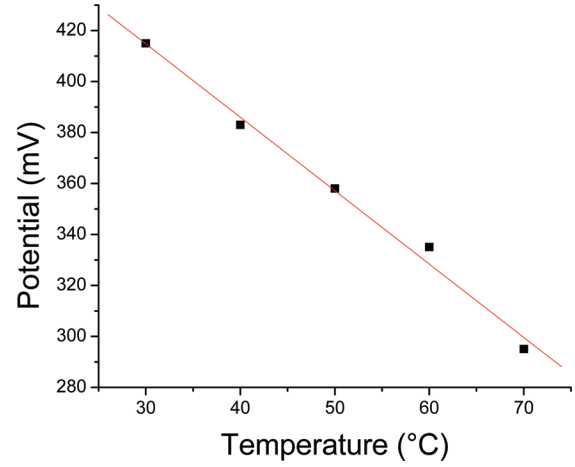

Figure 3. Potential at which CO begins to oxidize as a function of temperature.

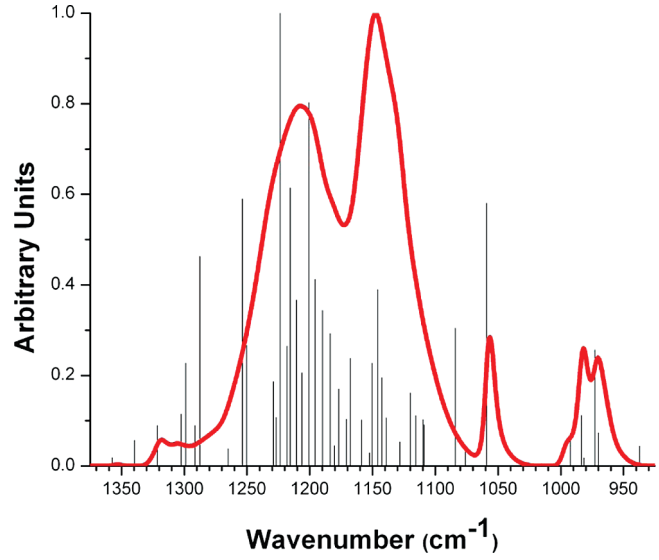

Figure 4. DFT calculated normal modes (black lines) and Nafion ATR spectrum (red).

Analysis of IR Spectra. The DFT calculated spectrum of a 55-atom Nafion side-chain and backbone segment provides 159 normal-mode frequencies and intensities. Figure 4 shows the theoretically derived peak positions and intensities (black lines) superimposed upon the ATR spectrum (red line) of hydrated Nafion.

PM-IRRAS enhances (relative to the ATR) vibrational modes of functional groups ordered by the Pt surface. Figure 5 shows the ATR spectrum (red), the PM-IRRAS spectra of the Nafion-H/Pt interface (gray line) and the Nafion-Li/Pt interface of Li^+ exchanged Nafion (blue line), and six selected (from the 159 calculated) DFT calculated frequencies and intensities.

Scheme 1 is the Nafion structure with functional groups labeled for ease of discussion. The low-frequency ATR band (Figure 5) at 971 cm^{-1} (corresponding to theoretical 984 cm^{-1}; line 1) and the 1056 cm^{-1} band (corresponding to theoretical 1059 cm^{-1}; line 3) have recently been thoroughly assigned by

(23) Persson, B. N. J.; Ryberg, R. *Phys. Rev. B* **1981**, *24*, 6954.

(24) Bard, A. J. *J. Am. Chem. Soc.* **2010**, *132*, 7559.

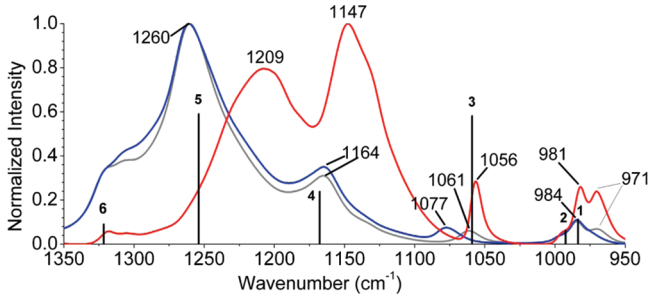

Figure 5. Theoretical and experimental spectra. ATR of hydrated Nafion (red); PM-IRRAS of Nafion-H on Pt (gray); PM-IRRAS of Nafion-Li on Pt (blue); Selected DFT peaks (black lines 1−6).

Scheme 1. Segment and Atom Labeling for Nafion

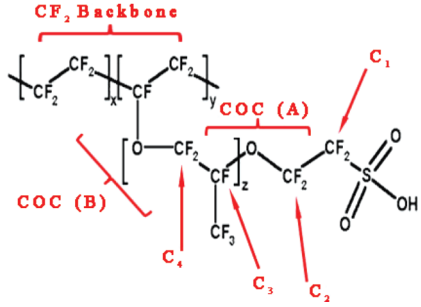

Webber et al.[25] They obtained high resolution transmission spectra of hydrated and thoroughly dehydrated Nafion and analyzed them in the context of the spectroscopy of the short chain ionomer (formerly DOW membrane), the Nafion sulfonyl fluoride,[26] and the Nafion sulfonyl imide.[27] Animations of the DFT calculated internal coordinates reveal that the observed 1056 and 971 cm^{-1} peaks both have internal coordinates resulting from the mechanical coupling of the adjacent sulfonate and COC (A) ether link.[25] Thus these peaks shift concertedly with changes in the sulfonate environment. Consider the ATR and PM-IRRAS spectra of the protonic form of Nafion (Figure 5, gray line). The 1056 and 971 cm^{-1} peaks concertedly shift to higher frequencies in the PM-IRRAS because of the interaction of the sulfonate functional group with the Pt surface. A similar effect is observed with Li^+ exchange of the adsorbed Nafion (blue line).

A convention for correlating PM-IRRAS enhanced peaks to the calculated DFT peaks would enable identification of functional groups ordered by the Pt surface: The association of observed PM-IRRAS peaks with DFT peaks, assigned by visualization of mechanically coupled internal coordinates,[25,28] provides the basis for such a convention. Normal mode coordinate animations (generated by Maestro from DFT output files) explicitly show how neighbor functional groups (called out in Scheme 1) are mechanically coupled. The calculated internal coordinates are viewed in the context of calculated normal modes of relevant small molecules (e.g., triflic acid, CF_3OCF_3, 10-carbon CF_2 backbone, etc.) hereafter referred to as "pure modes," which serve as the basis elements for assigning DFT calculated normal modes associated with observed peaks. Figure 6 shows the assignments of the six selected DFT peaks and snapshots of the corresponding Maestro animations. The atoms contributing to the dominating motion (black circles) and the next most significant atom motions (dotted circles) comprise pure modes that form the basis for the assignments. An alternate strategy for determining the dominant mode is to consider the contribution to the potential energy surface on an atom by atom basis.[29] While this may change the selection of the dominant mode, it does not alter what pure modes contribute to the assignments. The correlation of the DFT to PM-IRRAS peaks (Figure 5) and the resulting assignments in terms of the mechanically coupled modes are tabulated in Table 1.

The pure mode peak assignments (Table 1) elucidate functional groups ordered by the Pt surface. Animations of the pure modes and the internal coordinates of the six selected peaks are in Movies 1−12 and Movies 13−18 respectively in the Supporting Information as.AVI files. The rationale for the key functional group assignments (Table 1) is supported by the overlap of the DFT calculated peak positions with the PM-IRRAS peaks. Consider the DFT and PM-IRRAS peaks in the context of the bulk-Nafion ATR and the report by Cable et al.[26] that the 1056 and 971 cm^{-1} peaks shift with alterations of the sulfonate group environment. The bulk ATR peak at 1056 cm^{-1} (red), the PM-IRRAS peak of protonated Nafion adsorbed on Pt (gray line) at 1061 cm^{-1}, and the PM-IRRAS peak of lithiated Nafion adsorbed on Pt (blue line) at 1077 cm^{-1} (Figure 5) confirm that Pt surface atoms induce frequency *shifts*, as do the extent-of-hydration[25] and ion exchange of Nafion.[26] Thus the PM-IRRAS enhances bulk-Nafion modes that are shifted due to functional group interactions with Pt. Less explicit than the 1056 cm^{-1} peak are PM-IRRAS peaks derived from bulk-Nafion modes that are convoluted within the Nafion ATR broad envelope region (1100−1300 cm^{-1}), in particular the 1164 and 1260 cm^{-1} PM-IRRAS peaks. Di Noto et al.[30] extensively deconvoluted the broad envelope region. Their resulting peak library includes 1148, 1245 cm^{-1}, which could be reconciled with an association of the DFT peaks (Figure 5, lines 4 and 5) with the *shifted* PM-IRRAS peaks at 1164 and 1260 cm^{-1}.

Nafion/Pt Adsorption Model. The animation of the theoretical peak at 1254 cm^{-1} (Figure 5, line-5), associated with PM-IRRAS peaks at 1260 cm^{-1} (blue and gray lines), suggests that the CF_3 internal coordinates dominate the normal mode. The insensitivity of the 1201 cm^{-1} peak, to ion exchange, suggests that the internal coordinates are not substantially coupled to the sulfonate group. The 1260 cm^{-1} band intensity is over an order of magnitude greater than that of the cluster of peaks (i.e., associated with theoretical lines 1 and 2) that are mechanically coupled to the sulfonate pure mode: The CF_3 functional group is a coadsorbate of comparable importance to the sulfonate exchange group in the formation of the Nafion/Pt interface. Further support for this model is provided by Mulliken population[31] analysis. Atomic charges of the 55 Nafion fragment atoms were calculated. Table 2 shows the average charges of the backbone, side chain, and CF_3 group fluorine atoms and the average charges on the sulfonate oxygen atoms. The charges for chemically equivalent atoms (e.g., CF_3 fluorine and sulfonate oxygen atoms) differ because the calculations are done for the

(25) Webber, M.; Dimakis, N.; Kumari, D.; Fuccillo, M.; Smotkin, E. S. *Macromolecules* **2010**, *43*, 5500.
(26) Cable, K. M.; Mauritz, K. A.; Moore, R. B. *J. Polym. Sci., Part B: Polym. Phys.* **1995**, *33*, 1065.
(27) Byun, C. K.; Sharif, I.; DesMarteau, D. D.; Creager, S. E.; Korzeniewski, C. *J. Phys. Chem. B* **2009**, *113*, 6299.
(28) Warren, D. S.; McQuillan, A. J. *J. Phys. Chem. B* **2008**, *112*, 10535.
(29) Johansson, P. Chalmers University of Technology. *Personal Communication*, 2010.
(30) Di Noto, V.; Piga, M.; Lavina, S.; Negro, E.; Yoshida, K.; Ito, R.; Furukawa, T. *Electrochim. Acta* **2010**, *55*, 1431.
(31) Mulliken, R. S. *J. Chem. Phys.* **1955**, *23*, 1833.

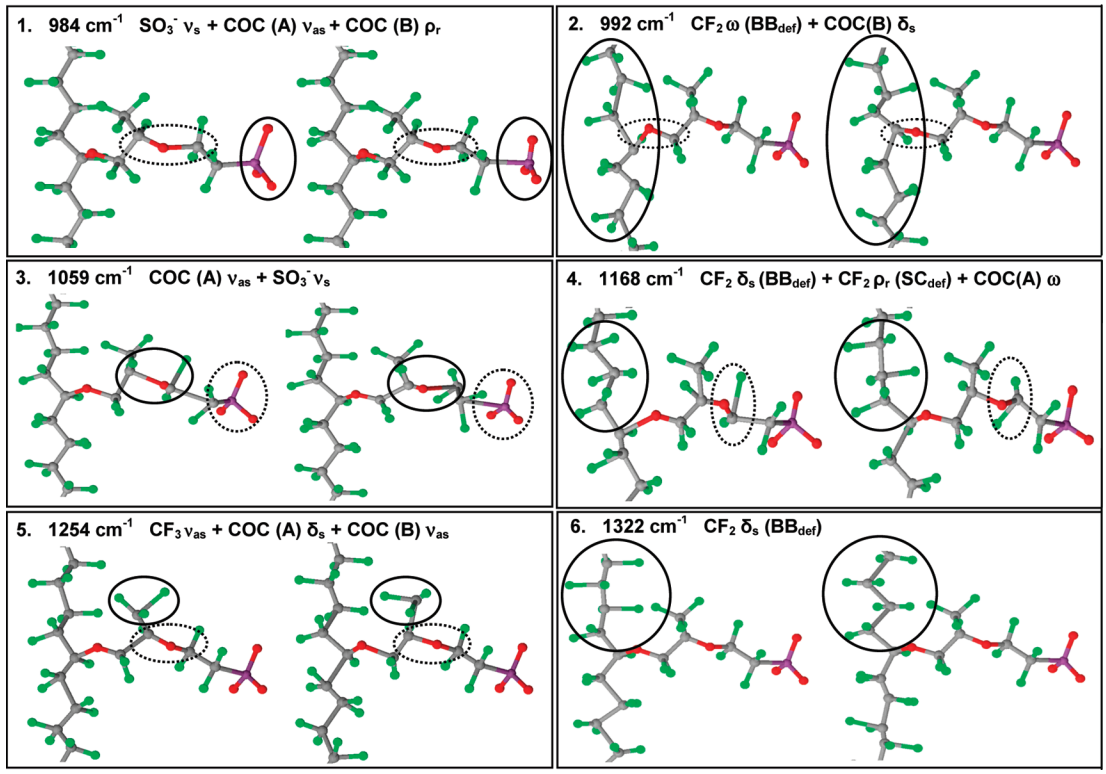

Figure 6. Normal mode coordinate animation snapshots of the Nafion side-chain anion and backbone fragment (see Scheme 1). Left and right views are extrema positions of the vibrational mode. Functional groups associated with the dominant internal coordinates and next most significant motions are designated by solid and dotted boundary lines respectively.

Table 1. PM-IRRAS and DFT IR Adsorption Peaks and Assignments[a]

	Wavenumber (cm^{-1})		
	PM-IRRAS	DFT	Pure Mode Components
1	971	984	SO_3^- $\boldsymbol{\nu}_s$ + COC(A) $\boldsymbol{\nu}_{as}$ + COC(B) $\boldsymbol{\rho}_r$
2	984	992	CF_2 $\boldsymbol{\omega}$ (**BB**$_{def}$) + COC(B) $\boldsymbol{\delta}_s$
3	1061	1059	COC(A) $\boldsymbol{\nu}_{as}$ + SO_3^- $\boldsymbol{\nu}_s$
4	1164	1168	CF_2 $\boldsymbol{\delta}_s$ (**BB**$_{stre}$) + CF_2 (**BB**$_{def}$) $\boldsymbol{\rho}_r$ + COC(A) $\boldsymbol{\omega}$
5	1260	1254	CF_3 $\boldsymbol{\nu}_{as}$ + COC(A) $\boldsymbol{\delta}_s$ + COC(B) $\boldsymbol{\delta}_s$
6	1322	1322	CF_2 $\boldsymbol{\delta}_s$ (**BB**$_{def}$)

[a] Symmetric stretch, ν_s; Asymmetric stretch, ν_{as}; Wagging, ω; Scissoring, δ_s; Twisting, τ; Rocking, ρ_r; Backbone deformation, BB_{def}; Side-chain deformation, SC_{def}; Backbone Stretching, BB_{stre}.

Table 2. Average Partial Charges of Selected Nafion Segments

Segment	Backbone (F) 13 atoms	Side chain (F) 8 atoms	CF_3 (F) 3 atoms	Sulfonate (O) 3 atoms
Avg Partial Charge	−0.0665	−0.0816	−0.0876	−0.4879
Standard Deviation	0.027	0.055	0.013	0.012

lowest energy Newman projections where the atomic environments are different for chemically equivalent atoms because of the absence of symmetry in the full molecule. The chemically equivalent atoms have smaller charge standard deviations as would be expected. The average charge of the CF_3 fluorine atoms are the highest among the three classes of fluorine atoms (Table 2) and are about 18% that of the sulfonate oxygens.

A Gaussian 03 Viewer (Gaussian, Wallingford, CT) used to construct a 2-equiv (1100 g/equiv) model of Nafion 117 enables rotation of dihedral angles while maintaining the native bond angles associated with each and every functional group. The CF_3 and SO_3^- groups, oriented with the two planes defined by the CF_3 fluorine and sulfonate oxygen atoms parallel to a Pt surface, effect ordering of the CF_2 backbone segments with respect to the Pt surface. Ordering of the CF_2 groups would be expected to yield PM-IRRAS peaks. The PM-IRRAS peak at 1164 cm^{-1} is associated with the theoretical peak (line-4) at 1168 cm^{-1}. The line 4 animation shows that CF_2 backbone internal coordinates dominate the 1168 cm^{-1} mode, supporting the suggestion of ordered CF_2 groups. Figure 7 is the Gaussian View model resulting from orienting the CF_3 and SO_3^- groups for adsorption to the Pt surface. The numbers (yellow) associate DFT calculated IR peaks (lines 1−6, Figure 5) and associated PM-IRRAS peaks with regions of order induced by the CF_3 and SO_3^- functional group adsorbates.

The ordering of the backbone CF_2 groups in the Gaussain model is a natural consequence of adjusting the dihedral angles of the anchoring groups for adsorption, while maintaining functional group native bond angles. Thus the aggregate of the Stark tuning data of Figure 2, the PM-IRRAS, and DFT calculations support Figure 7 as a model for Nafion functional group adsorption to Pt. The details of exactly how adsorbed CF_3 functional groups influence the operando Stark tuning curves is not yet established. The low density of functional group adsorption sites, relative to the number of backbone CF_2 groups, suggests an explanation as to why Nafion is observed to enhance electrode processes.[7,32] The methodology of assigning IR bands in the context of mechanically coupled internal coordinates of neighboring functional groups, and correlating those assignments

(32) Ploense, L.; Salazar, M.; Gurau, B.; Smotkin, E. S. *J. Am. Chem. Soc.* **1997**, *119*, 11550.

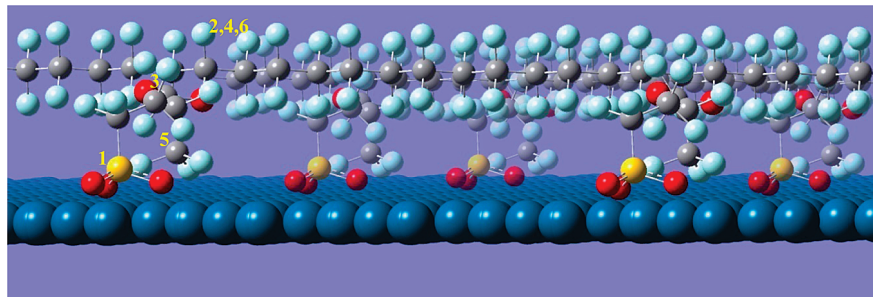

Figure 7. Gaussian 03 Viewer Nafion−Pt interface model. Oxygen (red), Sulfur (yellow), Fluorine (light blue), Carbon (gray), Pt (dark blue).

to functional groups interactions with metal surfaces, has broad applications toward characterization of ionomeric interfaces.

Conclusion

Operando IR spectroscopy, PM-IRRAS of Nafion−Pt interfaces, and ATR spectroscopy of Nafion, correlated with DFT calculated normal-mode frequencies, confirm that Nafion side-chain sulfonate *and* CF_3 coadsorbates are structural components of the Nafion−Pt interface. These "anchoring" functional groups reduce the degrees of freedom available for backbone and side-chain CF_2 dynamics. The partial ordering of Nafion CF_2 groups is supported by observed PM-IRRAS and DFT calculated peaks possessing vibrational internal coordinates dominated by, and mechanically coupled to, side-chain CF_2 group motions.

Acknowledgment. We thank the UT Pan American High Performance Computing Center. This work was funded by the Army Research Office and NuVant Systems Inc.

Supporting Information Available: AVI files of normal mode transitions (AVI file captions in PDF file). This material is available free of charge via the Internet at http://pubs.acs.org.

JA1081487

Operando X-ray and Infrared Spectroscopy of Polymer Electrolyte Fuel Cells

*Emily Lewis,† Ian Kendrick,† Qingying Jia,‡ Carlo U. Segre,‡ Eugene S. Smotkin† **

Department of Chemistry and Chemical Biology, Northeastern University, Boston MA 02115

Physics division, Department of Biological, Chemical and Physical Sciences, Illinois Institute of Technology, Chicago, Illinois, 60616

AUTHOR EMAIL ADDRESS: e.smotkin@neu.edu

Abstract: A cell design that enables both transmission and X-ray absorption spectroscopy of fuel cells, operating at temperature with flowing reactant streams, is used for operando spectroscopy of air breathing fuel cell cathodes catalyzed with PtNi and Pt. Fluorescence measurements enable signal-to-noise levels sufficient to study time-dependent edges at sub-mg/cm^2 on membrane electrode assemblies. Operando time and potential dependent XANES of a Pt catalyzed air breathing cathode show time constants for restructuring on the order of minutes to hours. The cell is designed for use for X-ray absorption spectroscopy for insertion into commercially available diffuse reflectance FTIR accessories.

KEYWORDS Fuel cell, membrane electrode assembly, operando spectroscopy, X-ray absorption spectroscopy, XAS

Manuscript Text:

Introduction: That the active state of a catalyst exists only during catalysis[1] is succinct rationale for *operando* (normal reactor conditions) characterization of catalytic devices. Polymer electrolyte

membrane reactors have applications in organic synthesis[2-4], environmental remediation[5] and energy conversion.[6] Operando characterization of flow reactor catalytic layers requires steady state reactant flow to the electrodes.

The membrane electrode assembly (MEA), a polymer electrolyte membrane (e.g. Nafion) sandwiched between electrode catalytic layers, is the heart of the reactor. The catalytic layers contact porous carbon paper or cloth diffusion layers optimized for reactant transport between the catalytic layers and the flow fields (grooves milled onto graphite plate surfaces). MEA fabrication methods have been reviewed.[7] Briefly; catalyst particles dispersed in solubilized Nafion (i.e. inks) are either deposited onto the diffusion layers and then hot pressed to the membrane (i.e. 5-layer membrane electrode assembly) or deposited onto a heated membrane surface (i.e. 3-layer membrane electrode assembly). The catalyst layers (carbon supported or metal blacks[8]) are a blend of ionomer, catalyst particles, and Teflon dispersion (at the cathode). The catalytic particles are coated with a sub-μm layer of ionomer that conducts protons and enhances catalysis.[9] The Nafion ionomer has sulfonate exchange sites that play a role in adhesion of the polymer to the catalytic surface.[10] Operando fuel cell operation requires an absence of supplemental electrolytes because aqueous electrolytes (e.g., H_2SO_4 or $HClO_4$) contribute mobile anion adsorbates *and* preclude fuel cell operation at the high end of relevant temperatures (e.g. 70-90 ^{o}C).

Proper cell design is the key challenge to operando spectroscopy. In addition to a "real world" catalyst environment, standard electrochemical cell design principles must be adhered to, including equal resistance between all points of the working electrode surface and the auxiliary electrode surface, and a low impedance reference electrode.[11] Proper selection of cell materials is crucial: Stainless steel includes iron, nickel and chromium, which fluoresce at energies similar to the edge energies of Pt based catalysts. Although challenging, these requirements are prerequisite to meaningful catalyst characterization.

Viswananthan[12] and Stoupin[13] introduced operando x-ray absorption spectroscopy of hydrogen and liquid feed direct methanol fuel cells respectively using the cell in figure 1. This cell design was

used by Principi[14] in low Pt loading x-ray adsorption spectroscopy (XAS) studies. Palladium at the cathode mitigates interference when studying Pt based catalyst edge energies.

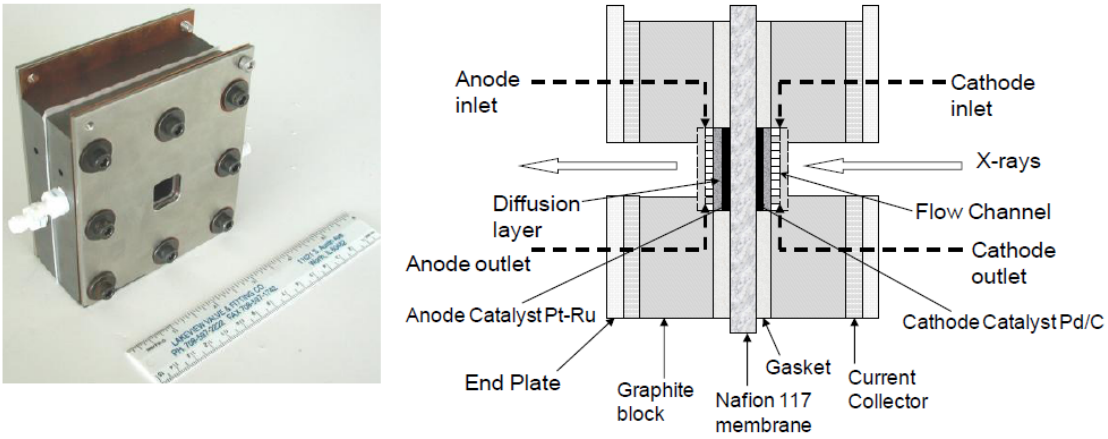

Figure 1. Operando spectroscopy fuel cell and schematic (from ref. 12)

The resistance between the anode and cathode catalytic layers of a membrane electrode assembly is governed by a fortuitously uniform polymer electrolyte membrane thickness (ca. 7 mil for Nafion 117).[15] The electrode counter to the working electrode of interest serves as both the auxiliary and the reference electrode (counter-reference electrode).[16] A hydrogen counter-reference is ideal for acquisition of direct methanol fuel cell anode polarization curves.[17] Pure water can be delivered to the counter-reference electrode when obtaining anode polarization curves because evolved hydrogen immediately poises[18] the counter-reference: The hydrogen ion activity is set by the Nafion weight Nafion (e.g. 1100 g for Nafion 117). The high acidity of Nafion is attributed to the CF_2 group alpha to the sulfonic acid exchange group.[19] Within the kinetically controlled region of the fuel cell polarization curve, the hydrogen electrode polarization is negligible. Although use of the counter-reference has drawbacks at high currents, the alternative of developing a 3rd electrode as a reference electrode is far more complex than correcting for reference electrode polarization losses using current interrupt or impedance measurements. On a practical level, the use of the fuel cell counter-reference affords greater reproducibility between laboratories.

Figure 2 shows the x-ray absorption near edge structure (XANES) spectra of Johnson Matthey PtRu black on the anode of the liquid feed fuel cell shown in figure 1. In the Pt L_{III}-edge data (left side),

the red line shows the operando Pt XANES at 450 mV, while the green and blue lines are the as-received catalyst (mounted on scotch tape), and Pt foil XANES respectively, also measured in transmission.

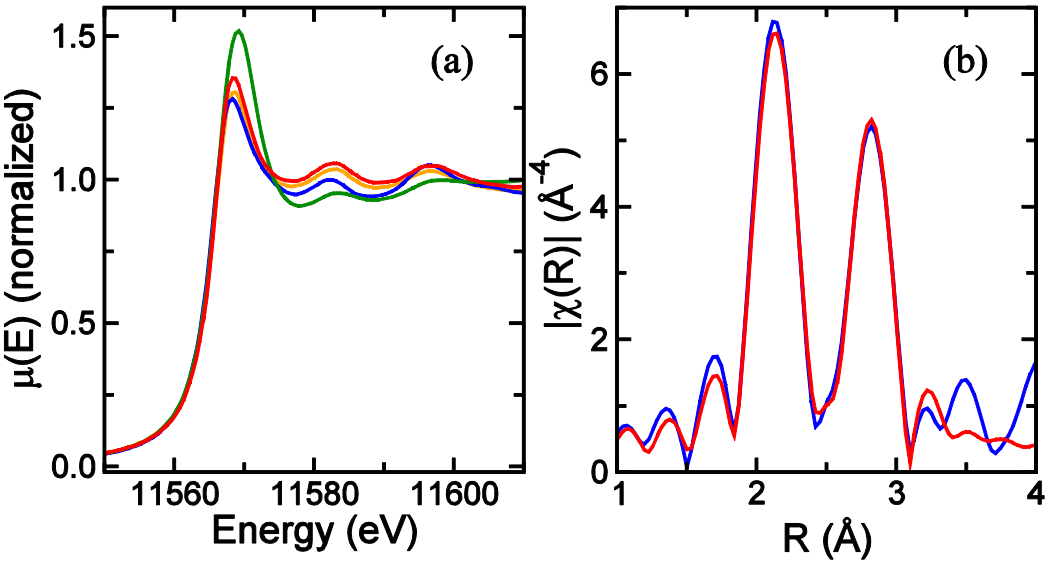

Figure 2 Left: Pt LIII-edge XANES: In situ catalyst at 450 mV (red), in situ catalyst at 450 mV from another run (orange), Pt foil (blue), and as-received catalyst (green). Right: Pt EXAFS fit (red line) to in situ catalyst data at 450 mV (blue) as a totally metallic environment (only Pt and Ru nearest neighbors). Fit range: 1.5 to 3.1 Å. (from ref. 13).

The increased white line intensity of the alloyed Pt (red) versus the pure Pt (blue) is due to alloy-induced d-band vacancies,[23] as was observed in XANES from an arc-melted PtRu 80:20 alloy.[24] The large edge intensity of the green curve confirms extensive oxidation of the as-received catalyst. Stoupin et al. observed that the potential-dependent (250, 300, 350, 400, and 450 mV) EXAFS perfectly overlap, confirming that, within the direct methanol fuel cell potential window, the Pt signal is insensitive to potential, similarly to the Pt within supported PtRu catalyst in a H_2/air fuel cell (i.e. Pt is metallic). Figure 2b shows the excellent first shell fit of the 350 mV EXAFS data (blue) with a model fit (red) simulating a totally metallic environment (fit range 1.5 to 3.1 Å) of mixed Pt and Ru atoms. Figure 3 shows the ex situ Ru K-edge XANES of metallic Ru powder (blue), in situ catalyst Ru at 350 mV (red), as-received PtRu (1:1) catalyst (green), Ru oxide (black), and Ru oxide hydrate (pink). As mentioned vide ante the above support the need for operando characterization.

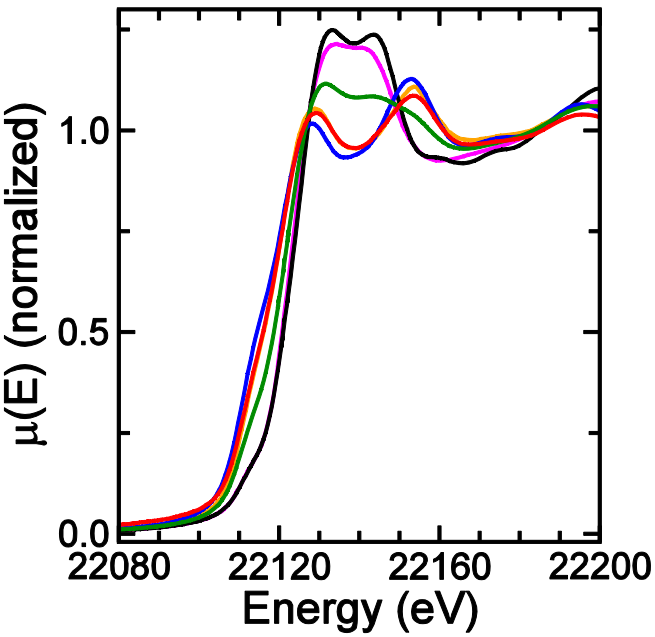

Figure 3 Ru K-edge XANES: Operating fuel cell anode at 450 mV (red, and orange another similar experiment), metallic Ru powder (blue), Ru oxide hydrate, (pink), Ru oxide (black), and as-received JM PtRu (1:1) (green) standards mounted on scotch tape. (from ref. 13).

The coincidence of the catalyst Ru edge at 350 mV (red) with the metallic Ru powder (blue) confirms that within direct methanol fuel cell operating potentials the Ru is primarily metallic. The deviation of the red from the blue line at 22,120 eV reflects the difference between the nearest-neighbor environments of pure Ru (hexagonal) and Ru in a Pt alloy FCC lattice. The as-received catalyst edge (green) is intermediate in energy between the metallic (blue and red) lines and the oxides of Ru (pink and black) confirming that the as-received catalyst is substantially oxidized. The near edge data of the as-received catalyst is intermediate between the saddle point of the Ru oxide and the metallic catalyst line (red), again confirming a substantially oxidized as-received catalyst.

A number of operando x-ray absorption[25-30] studies have followed with many focused on the oxidation state of the metal components. All found that at relevant fuel cell anode operating potentials, platinum is metallic. The oxidation of CO was studied both on Pt[29], and PtRu[25],[28, 31] [32] confirming the electronic benefits of Ru as a co-catalyst for CO oxidation. Studies of adsorbed oxygen

reduction reaction intermediates on fuel cell catalysts show that adsorption is both potential-dependent and site-specific.[25, 33-35]

Cell design: The Viswananthan cell could accommodate *both* transmission and fluorescence measurements under operando conditions. The new cell (Fig. 4) combines features of the Viswananthan cell[12] with the operando specular reflectance infrared cell reported by Fan et al.[39] This IR-XAS cell enables operando x-ray absorption spectroscopy (in transmission and fluorescence) and specular reflectance FTIR spectroscopy without the need for extraction of the MEA and interchange of cells. The top flow field, 2nd layer from top (Fig. 4 top), accommodates a CaF_2 window for IR reflectance studies.[39-41] The CaF_2 window can be removed when the working electrode of interest is an air breathing electrode. An advantage of fluorescence x-ray absorption is that beam intensity is not attenuated by the lower graphite flow field (4th layer from top). The IR-XAS cell is designed to interface to commercially available diffuse reflection accessories for FTIR systems (fig. 4, center). Figure 4 (bottom right) shows the lower flow field, the top flow field (with wicking material for removal of condensed water at the cathode) and the top plate for securing the CaF_2 window when used for IR reflectance.

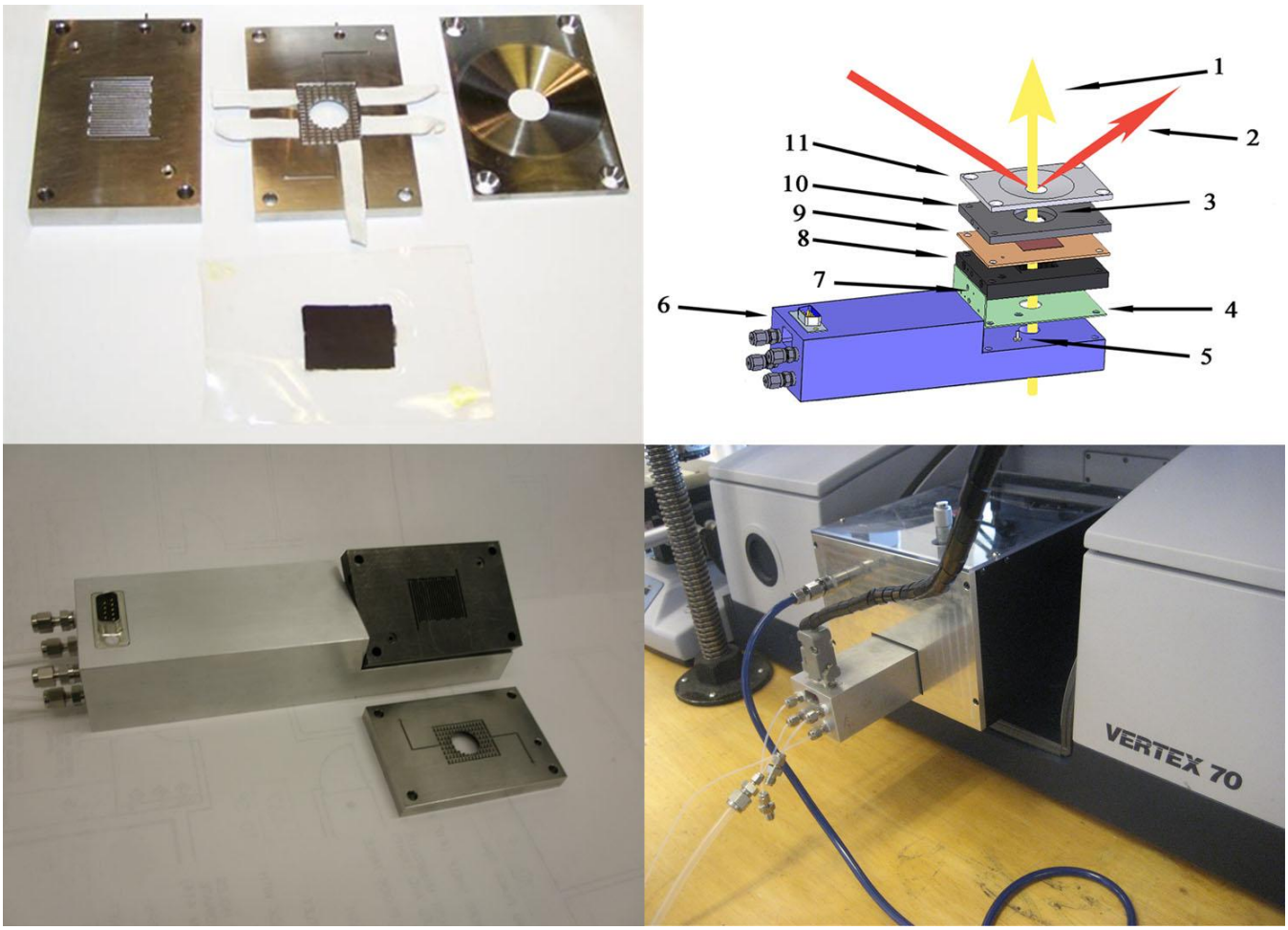

Figure 4 IR-XAS cell. Top left: Red path, reflectance IR or fluorescence XAS; yellow path; transmission XAS. Bottom left: Assembled spectroscopy cell with DE9 connector for electrodes, heater cartridge and thermister. Bottom right: Cell installed in Pike diffuse reflectance accessory in a Bruker (Billerica, MA) Vertex 70 FTIR Spectrometer. Bottom right: Bottom and top flow field with wicking material (white strips) adhered to upper flow field. MEA at bottom.

The fuel cell housing bolts to the slider assembly (blue component, fig. 4, top) which provides a 9-pin connector for cell electronics and temperature control. Swagelok fittings for fuel and oxidant are at the terminal end of slider assembly. A wide bevel (not viewable) within a slot underneath the cell (Fig. 4, bottom left) enables variable angles for transmission spectroscopy. Figure 5 shows the cell as an air breathing fuel cell at the MRCAT beamline at the Argonne National Laboratory. The source beam (red line) passes through the cathode gas diffusion layer on the front face of the cell (Fig. 5 right photo). Fluorescence (yellow line) is detected by the Lytle detector.

The underside slot also enables precise positioning of the cell under the diffuse reflectance integrated mirrors of the DiffuseIR accessory (Pike Technologies, Madison, WI) (Fig. 4, bottom center). A 158º bevel angle on the top plate maximizes the collection of the scattered signal. A pin-style upper flow field optimizes flow distribution around the CaF_2 window inset. Figure 6 shows a polarization curve obtained using the IR-XAS cell.

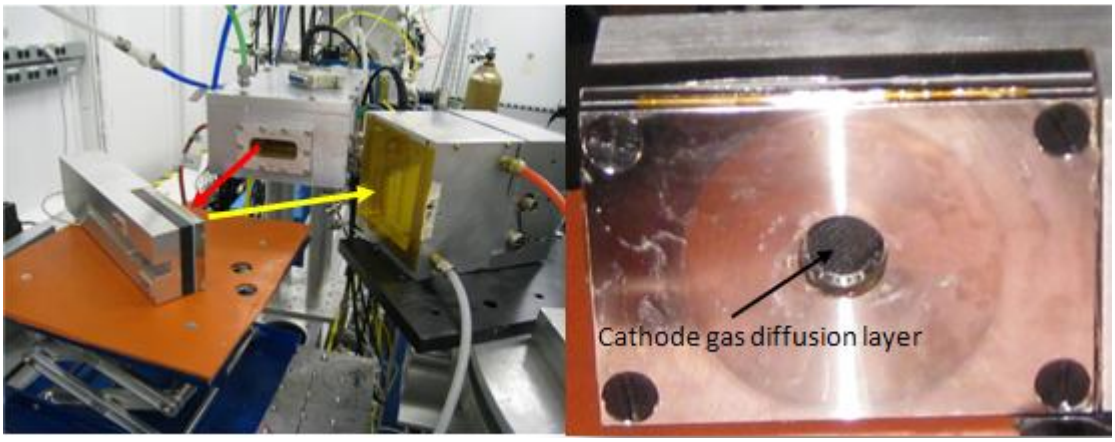

Figure 5 IR-XAS cell at MRCAT beamline, Argonne National Laboratory.

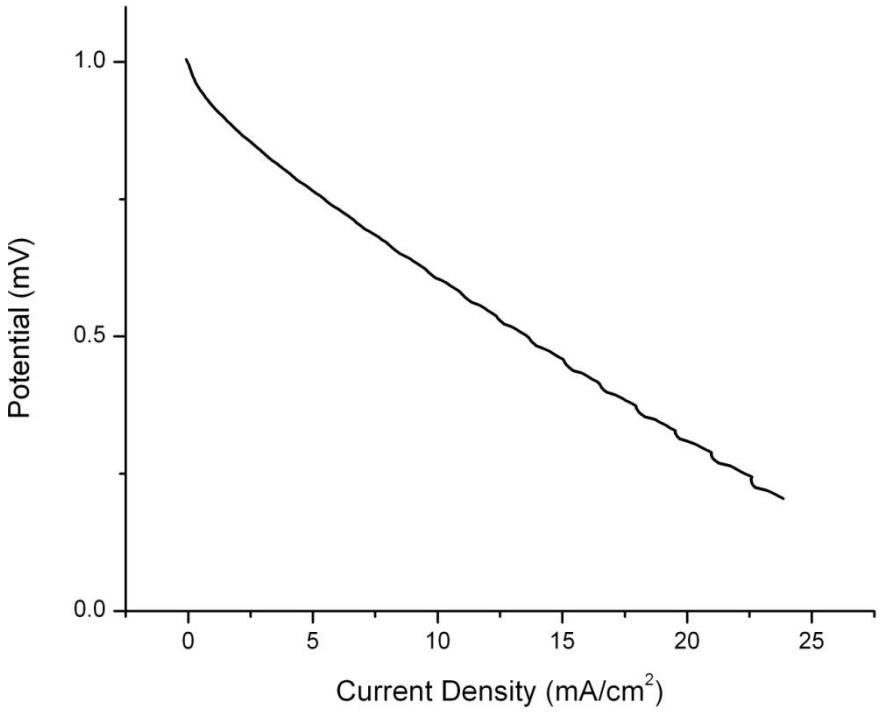

Figure 6. IR-XAS polarization curve.

Time dependent X-ray absorption spectroscopy: Figure 7- right shows subtractively normalized (XANES) spectra of a Johnson Matthey Pt cathode catalyst layer with the cell operating as a 50° C hydrogen-air fuel cell, including a spectrum of the dry MEA ex-situ. The cathode gas diffusion layer was exposed to ambient air (i.e. CaF_2 window not installed) while humidified hydrogen was delivered to the Pd counter-reference electrode. A reference XANES was obtained at 0 volts after a one-hour conditioning period,[42]. Potential dependent XANES were then sequentially acquired and subtractively normalized to the reference spectrum to yield Δμ fingerprints. At open circuit voltage, the white line intensity increases dramatically. The dry MEA fingerprint shows that the cathode is highly oxidized before exposure to the fuel cell environment, consistent with the results of Stoupin et al.[13]

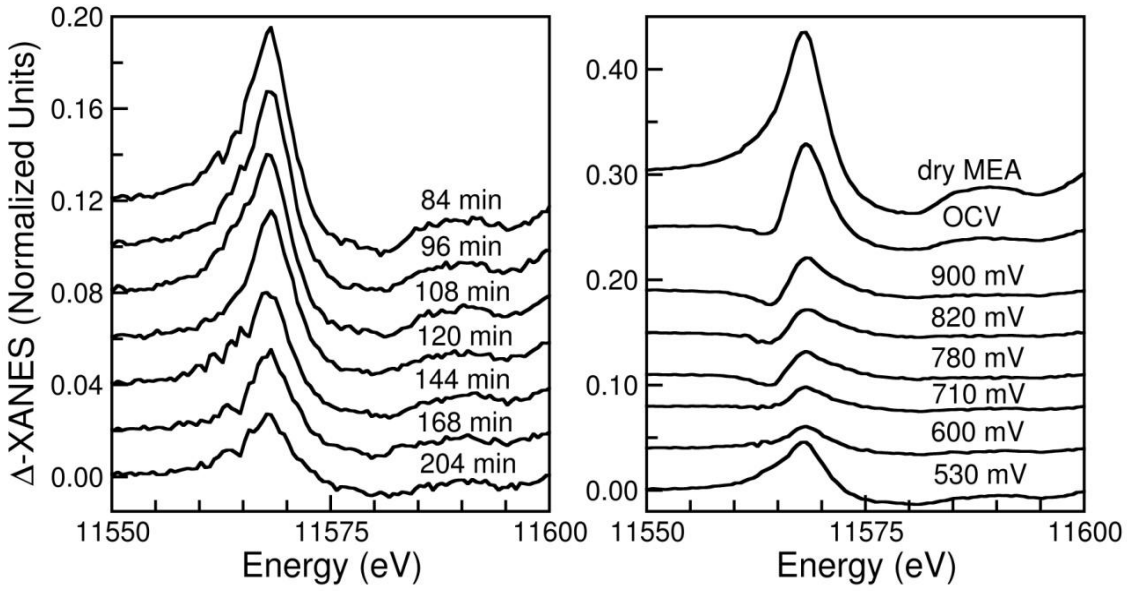

Figure 7. XANES of a Pt air-breathing cathode of the IR-XAS cell subtractively normalized to XANES at 0 volts vs. Pd hydrogen anode. Left: time dependent data at 530 mV; Right: potential dependent steady state data.

Figure 7-left shows time-dependent Δμ (at 530 mV), each obtained as an average of three consecutive scans. The potential-dependent data are smoother than the time-dependent data because 30 scans were averaged at each potential dependent fingerprint). The Δμ peaks decrease with time, as the Pt is reduced, with a time-constant on the order of hours. The large time constant cannot be attributed

solely to reduction of chemisorbed oxygen. The reduction of sub-surface oxygen, native to the crystallite core structure, may be responsible for the long time-constant. Stoupin et al. have shown that in the case of PtRu, the oxide phase extends into the core of particle. The data of Figure 7 suggest that subtractively normalized XANES, with time and potential dependence, have enormous value for elucidation of trends.

The time constants associated with the XAS of the work are on the order of minutes to hours. Also important are time constants shorter than a few seconds. Tada et al.[44] have reported a method for obtaining 1s time resolved full EXAFS spectra from a fuel cell being cycled between 0.4 and 1.0 V. They have observed separate time constants for charging, discharging as well as the formation and dissociation of surface Pt-O bonds using a fuel cell design very similar to that of Viswananthan in transmission mode. Even shorter time constants will be possible using dispersive XAFS techniques and lifetime studies using catalysts kept in operation for hundreds of hours will become possible as operando fuel cell fuel cells become more available.

Operando Infrared Spectroscopy of CO/Pt: Catalyst inks, prepared by the method of Wilson, [45] were directly applied to Nafion (4 mg/cm^2 of Johnson Matthey Pt black at both electrodes) immobilized on a heated (70°C) vacuum table (NuVant Systems, Crown Point, IN). These loading are typical for liquid feed direct methanol fuel cells. Carbon paper (Toray Industries, Tokyo, Japan) blocked with Vulcan XC-72, was used as current collectors at both electrodes. The infrared specular reflectance spectra of CO adsorbed (CO_{ads}) on the MEA Pt at 50 ^{o}C were obtained versus the CO dosing potential. The MEA was conditioned by cycling from 800mV to 600 mV (40 mV/min) for five cycles with H_2 and air at 50 and 250 sccm respectively. After conditioning, air was purged from the cathode with N_2, followed by further conditioning of the electrode by cyclic voltammetry over the range 0-1.2V (100mV/s) for fifty scans. Stripping data was acquired by CO dosing of the working electrode for 15 minutes at the selected dosing potential. After purging N_2 (200 sccm) for 15 minutes, the potential was cycled from 0-1.2 V at 10 mV/s. Figure 8 shows background CV (red) and the CO stripping wave (blue). At 50 ^{o}C the CO stripping initiates at around 600 mV.

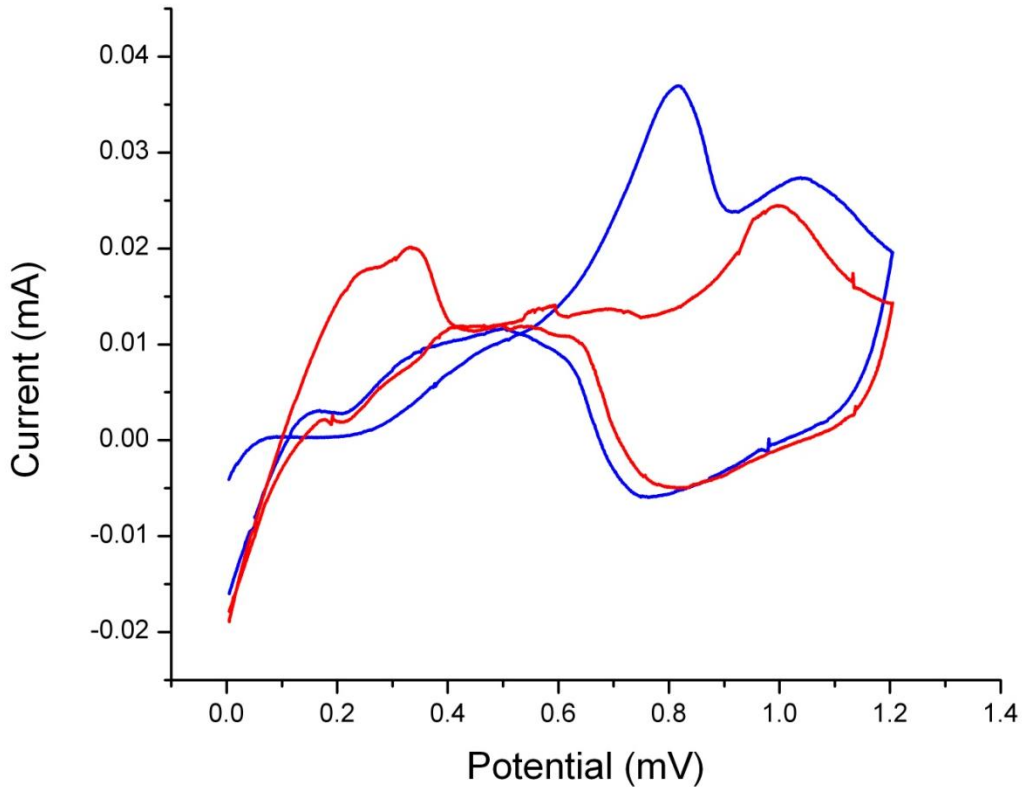

Figure 8. Cyclic voltammetry (10mV/s) of humidified N_2 fuel cell (5-cm^2 geometric) cathode; H_2 (50 sccm) at the counter-reference, at 50°C. CO stripping: blue; background; red.

Spectra over the range 800-4000 cm^{-1}, at 4 cm^{-1} resolution, were acquired on a Vertex 70 Spectrometer (Bruker instruments, Billerica, MA) using Opus 6.5™ analysis software. Prior to acquisition of the blank spectrum, the cell was brought 50 °C and was held at the desired potential. The flow rate of H_2 across the anode and N_2 across the cathode was 50 and 200 sccm respectively. The cell was allowed to equilibrate for five minutes before obtaining a blank. The cathode feed was switched to 40 sccm of CO at the desired potential for 15 minutes prior to purging the CO with N_2 (200 sccm). The potential was set to 100 mV prior to acquisition of four 250 signal averaged spectra at +50mV increments until the CO vibrational bands were no longer observable.

Stark tuning plots of CO adsorbed at 100, 200, 300 and 400 mV in the IR-XAS cell are shown in figure 9. The features of these plots include a linear region followed by a positive deviation from the

linear nature of the curve, a precipitous drop ending in a slight increase in slope. This study shows a correlation between the potential at which CO is adsorbed and the potential at which it begins to oxidize off of the electrode. As can be seen in figure 9, the lower the adsorption potential, the lower the potential at which CO begins to oxidize. This can be attributed to a lower amount of coverage due competitive adsorption of H_2 at the lower potentials.[46]

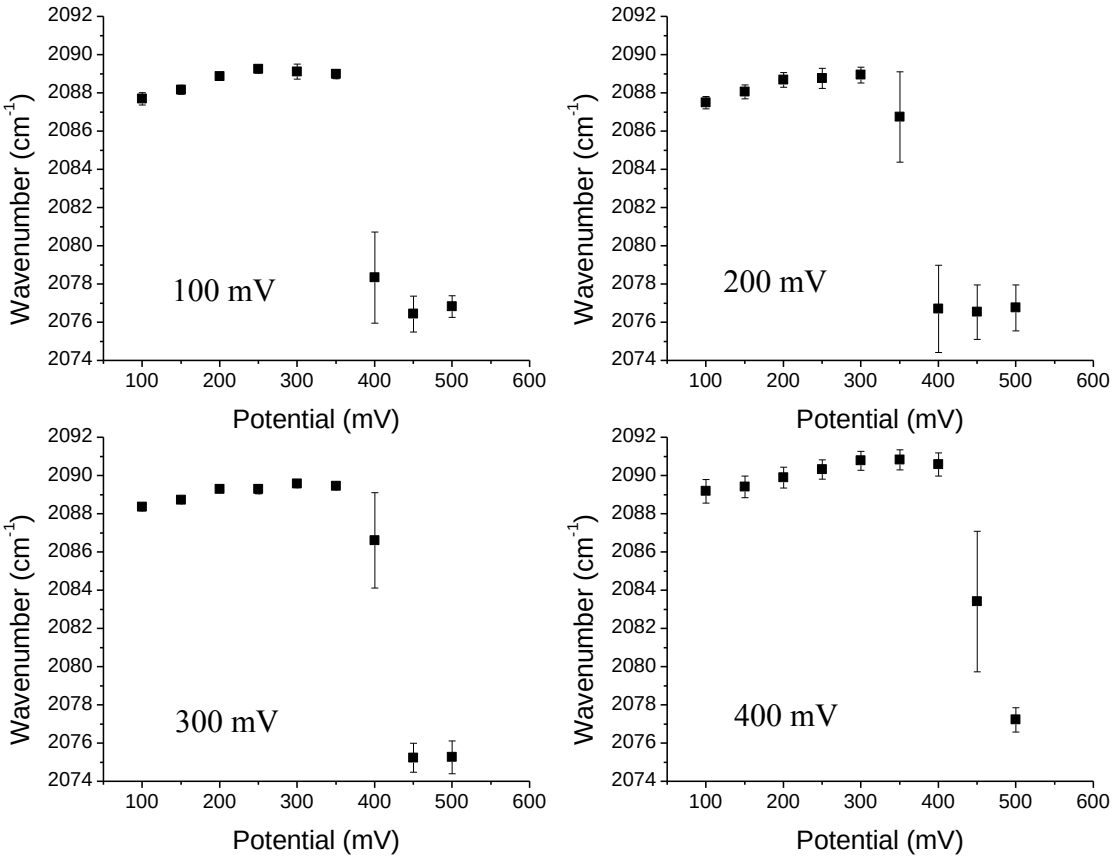

Figure 9. Stark tuning plots of linearly adsorbed CO adsorbed on Pt.

Markovic et al. [47] performed similar experiments using Pt(111) and 0.5 M H_2SO_4 and observed Stark tuning plots similar to those of Fig. 9. The increase in slope following the initial linear region was attributed the competitive adsorption of HSO_3^- generating a repulsive dipole interaction with CO. As OH^- begins to adsorb on the surface, CO is oxidized causing the shift of the CO vibrational peak to move to lower frequencies. The slight increase in wavenumber frequency at higher potentials is attributed to readsorption of HSO_3^-, reestablishing the repulsive dipole interaction. The observation that the behavior of the Stark tuning curve generated from the operando spectroscopy cell matches that from

an electrochemical cell using H_2SO_4 as an electrolyte despite the lack of mobile ions, suggests that Nafion adsorbs to the surface of the Pt electrode. This theory is supported by a study reporting on the Nafion-electrode surface interactions using polarization modulation-infrared reflection adsorption spectroscopy (PM-IRRAS) correlated with density functional theory (DFT).[10]

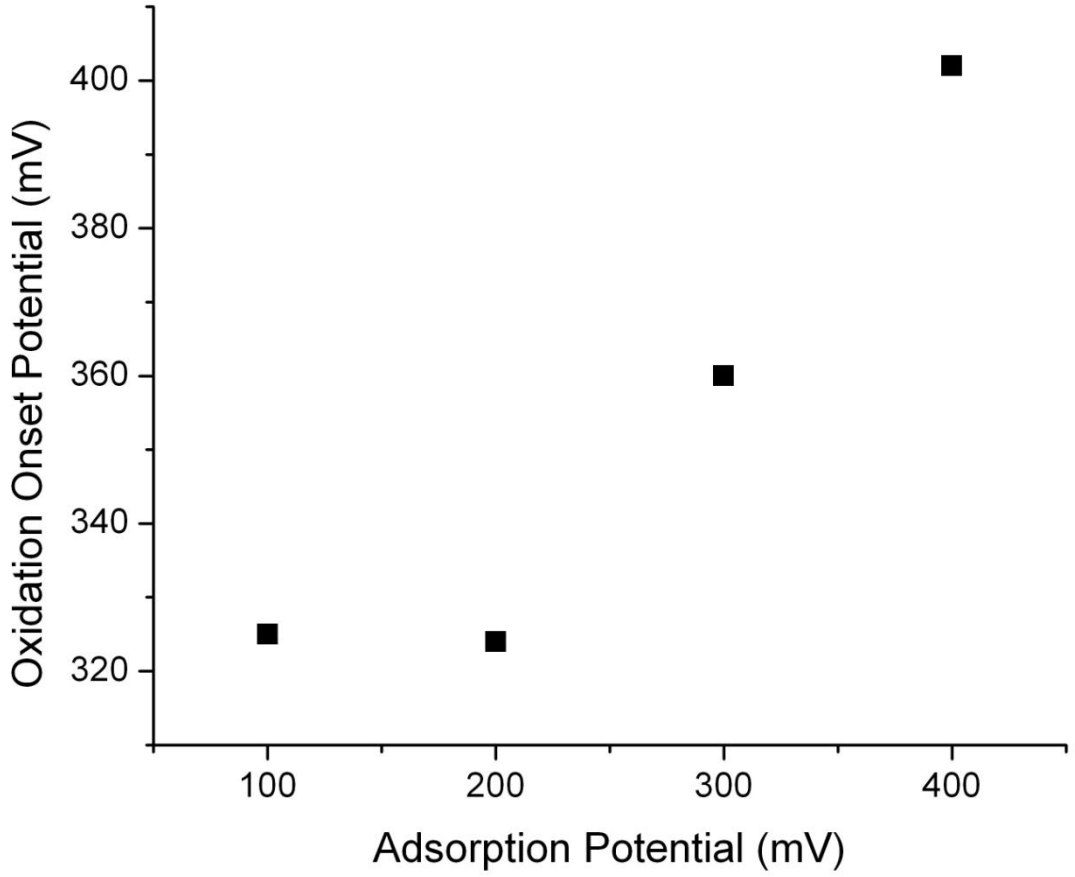

References

1. Topsoe, H., *Developments in operando studies and in situ characterization of heterogeneous catalysts.* Journal of Catalysis, 2003. **216**(1-2): p. 155-164.
2. Ploense, L., et al., *Proton spillover promoted isomerization of n-butylenes on Pd-black cathodes/Nafion 117.* Journal of the American Chemical Society, 1997. **119**(47): p. 11550-11551.
3. Ploense, L., et al., *Spectroscopic study of NEMCA promoted alkene isomerizations at PEM fuel cell Pd-Nafion cathodes.* Solid State Ionics, 2000. **136-137**: p. 713-720.
4. Salazar, M. and Smotkin, E.S., *Electrochemically promoted olefin isomerization reactions at polymer electrolyte fuel cell membrane electrode assemblies.* Journal of Applied Electrochemistry, 2006. **36**(11): p. 1237-1240.
5. Liu`, Z.`; Arnold`, R. G.`; Betterton`, E. A.`; Smotkin`, E.`, Reductive Dehalogenation of Gas-Phase Chlorinated Solvents Using a Modified Fuel Cell. Environmental Science & Technology 2001`, 35 (21)`, 4320-4326.

6. Smotkin, E.S. and Diaz-Morales, R.R., *New Electrocatalysts by Combinatorial Methods.* Annual Review of Materials Research, 2003. **33**(1): p. 557-579.
7. Gottesfeld, S. and Zawodzinski, T.A., *Polymer Electrolyte Fuel Cells*, in R.C. Alkire and D.M.K.a.C.W.T. H. Gerischer, Editors. 1997, Wiley-VCH. p. 229-244.
8. Liu, L., et al., *Carbon supported and unsupported Pt-Ru anodes for liquid feed direct methanol fuel cells.* Electrochimica Acta, 1998. **43**(24): p. 3657-3663.
9. Liu, L., et al., *Methanol oxidation on Nafion spin-coated polycrystalline platinum and platinum alloys.* Electrochemical and Solid-State Letters, 1998. **1**(3): p. 123-125.
10. Kendrick, I., et al., *Elucidating the Ionomer-Electrified Metal Interface*, in *J. Amer. Chem. Soc.* in press.
11. Kissinger, P.T. and Heineman, W.R., *Solution Resistance in Potentiostatic Circuits*, in *Laboratory Techniques in Electroanalytical Chemistry*. 1996, Marcel Dekker, Inc, New Yorki. p. 199.
12. Viswanathan, R., Liu, R., and Smotkin, E.S., *In situ x-ray absorption fuel cell.* Review of Scientific Instruments, 2002. **73**(5): p. 2124-2127.
13. Stoupin, S., et al., *Pt and Ru X-ray Absorption Spectroscopy of PtRu Anode Catalysts in Operating Direct Methanol Fuel Cells.* Journal of Physical Chemistry B, 2006. **110**(20): p. 9932-9938.
14. Principi, E., et al., *An XAS experimental approach to study low Pt content electrocatalysts operating in PEM fuel cells.* Phys Chem Chem Phys, 2009. **11**(43): p. 9987-95.
15. The first two digits are the equivalent weight of Nafion divided by 100`; the last digit is the thickness of Nafion in thousandths of an inch.
16. Rivera, H., et al., *Effect of sorbed methanol, current, and temperature on multicomponent transport in nation-based direct methanol fuel cells.* Journal of Physical Chemistry B, 2008. **112**(29): p. 8542-8548.
17. Gurau, B. and Smotkin, E., *Methanol crossover in direct methanol fuel cells: a link between power and energy density.* J. Power Sources, 2002. **112**: p. 339-352.
18. Bard, A. and Faulkner, L., *Electrochemical Methods: Fundamentals and Applications*. 2001: John WIley & Sons.
19. Buzzoni, R., et al., *Interaction of H2O, CH3OH, (CH3)(2)O, CH3CN, and Pryidine with the Superacid Perfluorosulfonic Membrane Nafion - An IR and Raman Study.* Journal of Physical Chemistry, 1995. **99**(31): p. 11937-11951.
20. Li, Q., et al., *The CO Poisoning Effect in PEMFCs Operational at Temperatures up to 200Â°C.* Journal of the Electrochemical Society, 2003. **150**(12): p. A1599-A1605.
21. Behm, R.J. and Jusys, Z., *The potential of model studies for the understanding of catalyst poisoning and temperature effects in polymer electrolyte fuel cell reactions.* Journal of Power Sources, 2006. **154**(2): p. 327-342.
22. Piela, P., et al., *Ruthenium Crossover in Direct Methanol Fuel Cell with Pt-Ru Black Anode.* Journal of the Electrochemical Society, 2004. **151**(12): p. A2053-A2059.
23. Mukerjee, S., Srinivasan, S., and Soriaga, M.P., *Role of structural and electronic properties of Pt and Pt alloys on electrocatalysis of oxygen reduction. An in situ XANES and EXAFS investigation.* Journal of the Electrochemical Society, 1995. **142**(5): p. 1409-22.
24. Viswanathan, R., et al., *In-Situ XANES of Carbon-Supported Pt-Ru Anode Electrocatalyst for Reformate-Air Polymer Electrolyte Fuel Cells.* Journal of Physical Chemistry B, 2002. **106**(13): p. 3458-3465.
25. Roth, C., et al., *Determination of O[H] and CO Coverage and Adsorption Sites on PtRu Electrodes in an Operating PEM Fuel Cell.* J. Am. Chem. Soc., 2005. **127**(42): p. 14607-14615.
26. Wiltshire, R.J.K., et al., *A PEM fuel cell for in situ XAS studies.* Electrochimica Acta, 2005. **50**(25-26): p. 5208-5217.

27. Roth, C., et al., *In-situ XAFS fuel cell measurements of a carbon-supported Pt-Ru anode electrocatalyst in hydrogen and direct methanol operation.* Physical Chemistry Chemical Physics, 2002. **4**(15): p. 3555-3557.
28. Scott, F.J., Roth, C., and Ramaker, D.E., *Kinetics of CO Poisoning in Simulated Reformate and Effect of Ru Island Morphology on PtRu Fuel Cell Catalysts As Determined by Operando X-ray Absorption Near Edge Spectroscopy.* J. Phys. Chem. C, 2007. **111**(30): p. 11403-11413.
29. Maniguet, S., Mathew, R.J., and Russell, A.E., *EXAFS of carbon monoxide oxidation on supported Pt fuel cell electrocatalysts.* Journal of Physical Chemistry B, 2000. **104**(9): p. 1998-2004.
30. Singh, J., et al., *In situ XAS with high-energy resolution: The changing structure of platinum during the oxidation of carbon monoxide.* Catalysis Today, 2009. **145**(3-4): p. 300-306.
31. Russell, A.E., et al., *In situ X-ray absorption spectroscopy and X-ray diffraction of fuel cell electrocatalysts.* Journal of Power Sources, 2001. **96**(1): p. 226-232.
32. Scott, F.J., Mukerjee, S., and Ramaker, D.E., *CO Coverage/Oxidation Correlated with PtRu Electrocatalyst Particle Morphology in 0.3 M Methanol by In Situ XAS.* Journal of The Electrochemical Society, 2007. **154**(5): p. A396-A406.
33. Teliska, M., O'Grady, W.E., and Ramaker, D.E., *Determination of H Adsorption Sites on Pt/C Electrodes in HClO4 from Pt L23 X-ray Absorption Spectroscopy.* J. Phys. Chem. B, 2004. **108**(7): p. 2333-2344.
34. Teliska, M., et al., *Site-Specific vs Specific Adsorption of Anions on Pt and Pt-Based Alloys.* J. Phys. Chem. C, 2007. **111**(26): p. 9267-9274.
35. Teliska, M., et al., *In situ determination of O(H) adsorption sites on Pt based alloy electrodes using X-ray absorption spectroscopy.* Proceedings - Electrochemical Society, 2005. **2003-30**(Fundamental Understanding of Electrode Processes): p. 212-216.
36. Bernardi, D.M., *Water-Balance Calculations for Solid-Polymer-Electrolyte Fuel Cells.* Journal of The Electrochemical Society, 1990. **137**(11): p. 3344-3350.
37. Bernardi, D.M. and Verbrugge, M.W., *Mathematical model of a gas diffusion electrode bonded to a polymer electrolyte.* AIChE Journal, 1991. **37**(8): p. 1151-1163.
38. Bernardi, D.M. and Verbrugge, M.W., *A mathematical model of the solid-polymer-electrolyte fuel cell.* Journal of the Electrochemical Society, 1992. **139**(9): p. 2477-91.
39. Fan, Q., et al., *In Situ FTIR-Diffuse Reflection Spectroscopy of the Anode Surface in a Direct Methanol/Oxygen Fuel Cell.* J. Electrochem. Soc., 1996. **143**(2): p. L21 - L23.
40. Bo, A.L., et al., *In situ Stark effects with inverted bipolar peaks for adsorbed CO on Pt electrodes in 50 degrees C direct methanol fuel cells.* Journal Of Physical Chemistry B, 2000. **104**(31): p. 7377-7381.
41. FTIR studies require a slot cut into the GDL to enable beam access to the catalytic surface.
42. Sanicharane, S., et al., *In situ 50 DegC FTIR spectroscopy of Pt and PtRu direct methanol fuel cell membrane electrode assembly anodes.* Journal of the Electrochemical Society, 2002. **149**(5): p. A554-A557.
43. Lewis, E.A., Segre, C.U., and Smotkin, E.S., *Embedded cluster -XANES modeling of adsorption processes on Pt.* Electrochimica Acta, 2009. **54**: p. 7181-7185.
44. Tada, M., et al., *In situ time-resolved dynamic surface events on the Pt/C catode in a fuel cell under operando conditions.* Angew. Chem. Int. Ed., 2007. **46**: p. 4310-4315.
45. Wilson, M.S. and Gottesfeld, S., *Thin-Film Catalyst Layers For Polymer Electrolyte Fuel-Cell Electrodes.* Journal of Applied Electrochemistry, 1992. **22**(1): p. 1-7.
46. Vidakovic, T., Christov, M., and Sundmacher, K., *The use of CO stripping for in situ fuel cell catalyst characterization.* Electrochimica Acta, 2007. **52**(18): p. 5606-5613.
47. Stamenkovic, V., et al., *Vibrational properties of CO at the Pt(111)-solution interface: the anomalous stark-tuning slope.* Journal of Physical Chemistry B, 2005. **109**(2): p. 678-680.

5500 *Macromolecules* **2010**, *43*, 5500–5502
DOI: 10.1021/ma100915u

Macromolecules
COMMUNICATION TO THE EDITOR

Mechanically Coupled Internal Coordinates of Ionomer Vibrational Modes

Matthew Webber,[†] Nicholas Dimakis,[‡] Dunesh Kumari,[†] Michael Fuccillo,[†] and Eugene S. Smotkin*,[†]

[†]*Department of Chemistry and Chemical Biology, Northeastern University, 360 Huntington Ave, Boston, Massachusetts 02115, and* [‡]*Department of Physics and Geology, University of Texas-Pan American, 1201 W University Dr., Edinburg, Texas 78539*

Received April 26, 2010
Revised Manuscript Received June 1, 2010

Nafion, a sulfonated tetrafluoroethylene copolymer, and its short-side-chain derivative revolutionized low-temperature fuel cell development. Nevertheless, after over 7000 publications on Nafion since 1975,[1] the definitive assignment of key infrared (IR) peaks, including those associated with the SO_3^- exchange group and the ether linkages, has been elusive. Nafion and relevant derivatives are given in Scheme 1.

The highlights of reported interpretations of selected IR spectra (Figure 1a−f) provide the context for this Communication. The attenuated total reflectance (ATR) spectra of hydrated Nafion (a) and the short-side-chain ionomer (b) (i.e., Scheme 1) focus on the ~1060 cm^{-1} and a multiplet that includes a shoulder at 995 cm^{-1} and two peaks ~983 and 970 cm^{-1}, hereafter referred to as $\bar{\nu}_{hf}$ and $\bar{\nu}_{lf}$, respectively. The $\bar{\nu}_{hf}$ and $\bar{\nu}_{lf}$ have been conventionally assigned to ether groups in proximity to the backbone and the sulfonate group, respectively. Cable et al.[2] associated $\bar{\nu}_{lf}$ to the ether linkage closest to the sulfonate group because of its enhanced sensitivity to ion exchange and the fact that the $\bar{\nu}_{lf}$ persists in the Dow short-side-chain ionomer spectrum. The short-side-chain ionomer has only one ether group, positioned adjacent to the sulfonate group. The sulfonyl fluoride precursor was also compared to Nafion. In the sulfonyl fluoride spectrum (c), $\bar{\nu}_{lf}$ diminishes concurrently with the ~1060 cm^{-1} peak. These observations were reconciled by invoking solvation effects as responsible for the sensitivity of $\bar{\nu}_{lf}$ to ion exchange because in hydrated Nafion, the sulfonate group is embedded in an aqueous phase. Therefore, the ether group in closest proximity to the sulfonate group may be subject to solvation as well and thus sensitive to ion exchange. The $\bar{\nu}_{hf}$, which is essentially insensitive to ion exchange, has been attributed to the ether link distant from the sulfonate group. Further, Cable[2] concluded that the concurrent loss of the 1060 cm^{-1} peak is due to the loss of the SO_3^- symmetric mode.

The association of the 1060 cm^{-1} peak and $\bar{\nu}_{lf}$, solely with SO_3^- and ether link modes, respectively, precludes proper analysis of the spectra. However, if the mechanical coupling of the internal coordinates of the SO_3^- and its near-neighbor COC are considered, the analysis of 1060 cm^{-1} and $\bar{\nu}_{lf}$ peaks of Figure 1 can be reconciled without the need for invoking solvation of the ether link (vide infra). Warren and McQuillan[3] noted the importance of the considering vibrational contributions from more than one functional group when assigning IR absorptions of fluoropolymers. Byun et al.[4] also reported the same loss of the $\bar{\nu}_{lf}$ upon substitution of the sulfonic acid group for a sulfonyl imide (spectrum f) and assigned $\bar{\nu}_{lf}$ as did Cable et al. (Figure 1e,f).

*To whom correspondence should be addressed.

Scheme 1. Structures of Nafion and Derivatives

R: -SO_3H (Nafion)
-SO_2F (sulfonyl fluoride)
-$SO_2N(H)SO_2CF_3$ (-sulfonyl imide)

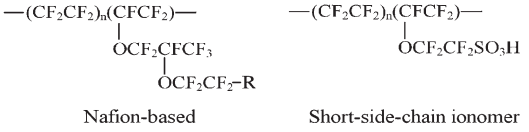

Nafion-based Short-side-chain ionomer

Transmission infrared spectra of Nafion 112 were obtained on a Bruker Vertex 80V spectrometer (Bruker Optics Inc., Billerica, MA) under dry air or vacuum. All spectra were an average of 100 scans. The Nafion samples were dehydrated on a vacuum line at 10^{-2} Torr (under nitrogen) at 135 °C for several hours. Samples were transferred to a drybox for sample holder installation in order to minimize atmospheric exposure. The transmission spectra (Figure 2) show a concurrent loss of intensity of 1062 cm^{-1} and $\bar{\nu}_{lf}$ due to dehydration of the membrane, simultaneous with evolution of peaks at 1415 and 908 cm^{-1}.

We attribute the transition of the dehydrated (red) to the hydrated (blue) spectrum to a change in the point group symmetry of the sulfonic acid group (vide infra). The following density functional theory (DFT) calculations show that as the proton dissociates from the sulfonic acid group (e.g., with hydration), the local point group symmetry changes from C_1 to C_{3v}.

Unrestricted DFT[5,6] with the hybrid X3LYP[7] functional was used for geometry optimization and calculations of the normal-mode frequencies and corresponding IR spectra of triflic acid, the Nafion side chain (NSC), and the NSC with a PTFE backbone segment (NSCB). The calculations were done at water/sulfonate ratios (λ)[8] from 0 to 10. The X3LYP extension of the B3LYP[9] functional yields more accurate heats of formation. The all-electron 6-311G**++ Pople triple-ζ basis set is used in all calculations ("**" and "++" denote polarization[10] and diffuse[11] basis set functions, respectively). Jaguar 6.5 (Schrodinger Inc., Portland, OR) uses the pseudospectral method[12] for calculation of time-consuming integrals with the same accuracy as the fully analytical DFT codes.

Images of the geometry optimized NSC and NSCB anion are shown in Figure 3.

Figure 4 shows DFT optimized structures of the triflic acid exchange site as water molecules are sequentially added. The option to include a dielectric in the calculation was not used because the effect of such an option would be a small perturbation over the effects due to sequential addition of water molecules to the solvation sphere. The triflic acid calculations reveal a threshold λ (λ_d) where the SO−H bond dissociates (Figure 4, top right), and a $\lambda_{i\text{-}o}$, where the H_3O^+ loses a direct hydrogen bond to the sulfonic acid anion (Figure 4, bottom right.) Paddison used B3LYP/6-31G** to calculate λ_d and $\lambda_{i\text{-}o}$ of 3 and 6, respectively.[13] Although different from our values of 4 and 10, respectively, the near-identical O−H and O−O distances support the converged energies of both Paddison and our calculations (see Table 1).

Our higher value of λ_d results from the use of diffuse basis set functions. Spitznagel et al.[14] observed significant changes to optimized geometries involving anions and proton affinity when using diffuse functions. To confirm the findings of Spitznagel,[14] the triflic acid structure was optimized for $\lambda = 3$ without diffuse functions, resulting in the same λ_d as Paddison. This provides confidence in our attribution to diffuse functions for a higher

 Published on Web 06/08/2010

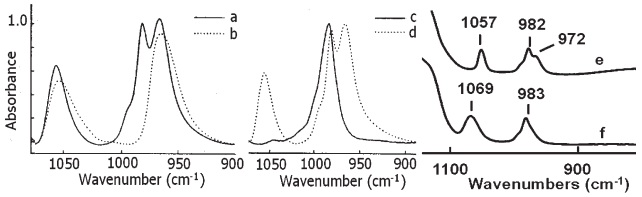

Figure 1. (a) Nafion-H, (b) short-side-chain ionomer, (c) sulfonyl fluoride, (d) Nafion-H, (e) H^+ form of Nafion, and (f) sulfonyl imide. Spectra a−d adapted from Cable et al.[2] Spectra e and f adapted from ref 4.

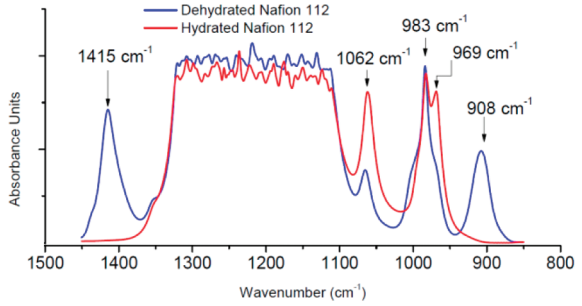

Figure 2. Transmission IR spectra of Nafion 112 showing the evolution of 1415 and 908 cm^{-1} bands upon dehydration.

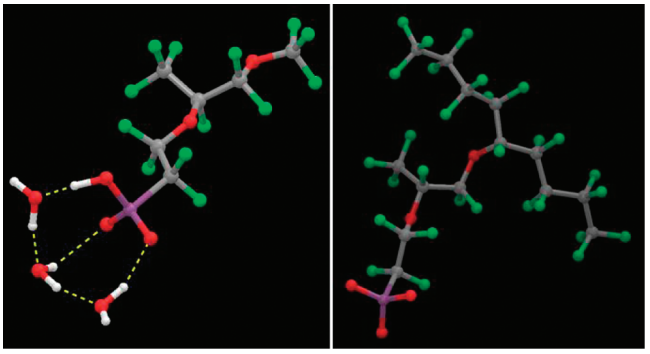

Figure 3. NSC $\lambda = 3$ (left); NSCB anion (right) (red = O, white = H, gray = C, purple = S, green = F, yellow dotted lines = H-bonds).

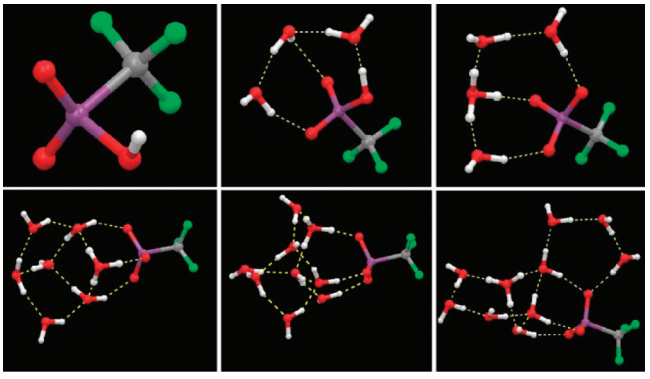

Figure 4. Proton dissociation threshold and the formation of H_3O^+ and C_{3v} local symmetry. Top: $\lambda = 0$, left; $\lambda = 3$, center; $\lambda = 4$, right. Bottom: $\lambda = 7$, left; $\lambda = 9$, center; $\lambda = 10$, right (red = O, white = H, gray = C, purple = S, green = F, yellow dotted lines = H-bonds).

value of λ_d. We attribute our higher value of $\lambda_{i\text{-}o}$ to the use of X3LYP, developed to significantly improve hydrogen bonding and van der Waals interactions over B3LYP.[7] A comparison to similar computational studies of trilfic acid λ_d and $\lambda_{i\text{-}o}$ values is summarized in the Supporting Information.[13,15−18]

Table 1. Comparison of the Acidic Proton O−H Distances and the O−O Distances about the Central Hydrogen Ion for Triflic Acid

	SO−H (Å)		SO−H−OH (Å)	
λ	Paddison[13]	present	Paddison[13]	present
0	0.973	0.970		
1	1.02	1.004	2.595	2.628
2	1.059	1.037	2.496	2.531
3	1.562	1.074	2.556	2.465
4	1.721	1.522	2.658	2.526
5	1.739	1.481	2.693	2.503
6	3.679	1.49	4.243	2.519
7		1.511		2.523
8		1.528		2.539
9		1.523		2.539
10		3.677		4.372

Table 2. Comparison of O−H Distance for the Acidic Proton and the O−O Distance to the Central Hydronium O (or Nearest Water Molecule)

	SO−H (Å)		SO−H−OH (Å)	
λ	triflic acid	NSC	triflic acid	NSC
3	1.074	1.077	2.465	2.464
4	1.522	1.531	2.526	2.541
7	1.511	1.526	2.523	2.533
9	1.523	1.532	2.539	2.545

Extension of the λ-dependent calculations to NSC confirms a $\lambda_d = 4$, consistent with the triflic acid calculations. NSC calculations at $\lambda = 7$ and 9 confirm a $\lambda_{i\text{-}o}$ greater than 9. The SO−H and SO−H−OH distances versus λ are presented in Table 2. The similarities between the O−H and O−O distances of solvated triflic acid and NSC, versus λ, suggests that at the levels of hydration calculated the sulfonic acid group behavior is rather generic.

Although hydrated Nafion has C_1 symmetry overall, it has regions of local symmetry, namely the $-SO_3^-$ (C_{3v}) and the ether groups (C_{2v}). Maestro (Schrodinger Inc., Portland, OR) converts Jaguar output files to vibrational mode animations. The full animations of selected calculated modes are in the Supporting Information. Snapshots of the $CF_3SO_3^-$ symmetric stretch ($\nu_s(A_1)$) and the CF_3OCF_3 asymmetric ($\nu_{as}(B_2)$) and rocking modes ($\rho_r(B_2)$) and associated frequencies are shown (Figure 5, top row).

Hereafter, the $\nu_s(A_1)$, $\nu_{as}(B_2)$, and $\rho_r(B_2)$ modes are referred to as "pure modes". The equilibrium positions and vibrational mode extrema of NSCB modes corresponding to the bands at 969 cm^{-1} ($\bar{\nu}_{lf}$) and 1060 cm^{-1} (Figure 2) are shown in Figure 5. The animations enable visualization of how the pure mode internal coordinates mechanically couple to yield the NSCB modes. The center row snapshots show a 983 cm^{-1} NSCB mode[20] that results from the coupling of the $\nu_s(A_1)$, $\nu_{as}(B_2)$, and $\rho_r(B_2)$ with the dominate mode being the $\nu_s(A_1)$. The full animations show that the dominate pure mode of the 1060 cm^{-1} peak is actually the CF_3OCF_3 $\nu_{(as)}(B_2)$ mode with a much weaker contribution from the $\nu_s(A_1)$ of triflic acid. The 1060 cm^{-1} is primarily a $\nu_{as}(B_2)$ mode mechanically coupled to the internal coordinates of the $\nu_s(A_1)$ of the SO_3^- group. The key point is that the ether link nearest the exchange group has internal coordinates that are mechanically coupled to the $\nu_s(A_1)$ mode: The 1060 cm^{-1} and $\bar{\nu}_{lf}$ peaks cannot be purely ascribed to the SO_3^- and COC modes, respectively.

In fact, ν_{lf}, conventionally assigned as an ether mode, derives from the triflic acid SO_3^- $\nu_s(A_1)$ mode with a calculated average of 974 cm^{-1} (see Table 3).

The above analysis obviates the need to invoke ether link solvation for analysis of the Figure 1 spectra. Because the internal coordinates of the 1060 cm^{-1} and ν_{lf} peaks are mechanically

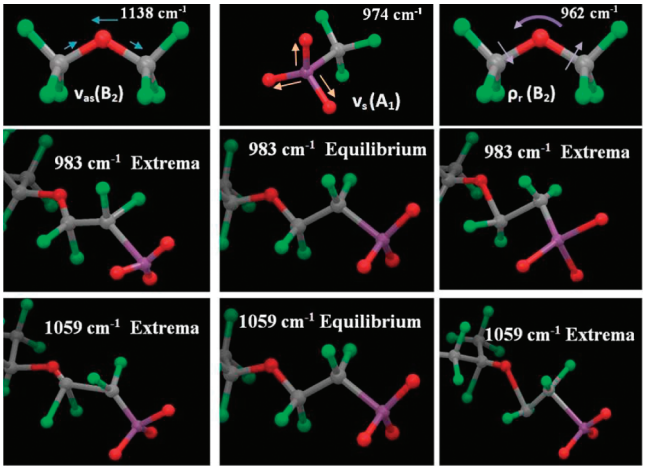

Figure 5. Maestro animation snapshots of DFT calculated modes of the full side chain and backbone: (top row) small molecule "pure" modes; (middle row) 983 cm^{-1}, equilibrium positions in center panel; (bottom row) 1060 cm^{-1}, equilibrium positions in center panel. Extrema at left and right panels of center panels. AVI animations are given in the Supporting Information.

Table 3. Calculated $\nu_s(A_1)$ Mode of C_{3v} (i.e., λ_d or Greater) Sulfonate

	triflic acid SO_3^- sym str (cm^{-1})		triflic acid SO_3^- sym str (cm^{-1})
$\lambda = 4$	978	$\lambda = 8$	979
$\lambda = 5$	965	$\lambda = 9$	980
$\lambda = 6$	980	$\lambda = 10$	975
$\lambda = 7$	964		

coupled, *they always shift* (*upon ion exchange of the SO_3^- group*) *or diminish together* (*upon dehydration,* Figure 2).

Reconsider the spectra of Figure 1 in light of mechanically coupled internal coordinates. The $\bar{\nu}_{hf}$ is not in the short-side-chain spectra (b) because $\bar{\nu}_{hf}$ was the backbone ether link that was not mechanically coupled to the SO_3^-. In the short-side-chain derivative, the remaining $\bar{\nu}_{lf}$ is now the backbone ether link mechanically coupled to the SO_3^- group (i.e., the functional groups responsible for the mechanically coupled $\nu_s(A_1)$, $\nu_{as}(B_2)$, and $\rho_r(B_2)$ are now in close proximity to the backbone). In the sulfonyl fluoride spectra (c), the C_{3v} symmetry of the SO_3^- is lost.

Thus, similar to the case of dehydration (Figure 2), the $\bar{\nu}_{lf}$ and 1060 cm^{-1} peaks vanish. The sulfonyl imide spectra (f) behaves similarly to that of the sulfonyl fluoride. The remaining peak at 1069 cm^{-1} is not inconsistent with our analysis. Korzeniewski confirmed this peak as the asymmetric S−N−S stretch.

Warren and McQuillan[3] recognized that Nafion vibrational modes have contributions from multiple functional groups using DFT at the B3LYP/6-311G+(d,p) level of theory. Their calculated 929 cm^{-1} mode was assigned to a coupling of C−S stretching and SO_3^- symmetric stretching to explain the loss of the 971 cm^{-1} band upon dehydration. Okamoto[19] calculated peaks at 989 and 1060 cm^{-1} as SO_3^- symmetric and COC (nearest the headgroup) asymmetric stretching, respectively, for a model side chain of Nafion in its anion form, $(CF_3)_2CFOCF_2CF(CF_3)$-$OCF_2CF_2SO_3^-$, using B3LYP/6-31G(d,p)++.

The 1060 cm^{-1} and $\bar{\nu}_{lf}$ peaks result from the mechanical coupling of the internal coordinates of SO_3^- and the COC "pure" modes. The 1060 cm^{-1} mode is dominated by an ether link mode. The calculated mode at 983 cm^{-1}, a major contributor to the $\bar{\nu}_{lf}$ peak, is dominated by the SO_3^- $\nu_s(A_1)$ mode. The consideration of mechanically coupled internal coordinates is essential for the analysis of infrared spectra of ionomers and correlation of those spectra with the effects of ion exchange and state of hydration.

Acknowledgment. We thank the UT Pan American High Performance Computing Center and comments from reviewer #1 and Max Diem. Funding was provided by ARO DURIP W911NF-07-1-0236.

Supporting Information Available: Maestro animations and summary table of proton dissociation studies. This material is available free of charge via the Internet at http://pubs.acs.org.

References and Notes

(1) ISI Web of Knowledge Home Page, **2009**; Vol. *2009*.
(2) Cable, K. M.; Mauritz, K. A.; Moore, R. B. *J. Polym. Sci., Part B: Polym. Phys.* **1995**, *33*, 1065.
(3) Warren, D. S.; McQuillan, A. J. *J. Phys. Chem. B* **2008**, *112*, 10535.
(4) Byun, C. K.; Sharif, I.; DesMarteau, D. D.; Creager, S. E.; Korzeniewski, C. *J. Phys. Chem. B* **2009**, *113*, 6299.
(5) Hohenberg, P.; Kohn, W. *Phys. Rev. B* **1964**, *136*, 864.
(6) Kohn, W.; Sham, L. J. *Phys. Rev. A* **1965**, *140*, 1133.
(7) Xu, X.; Zhang, Q. S.; Muller, R. P.; Goddard, W. A. *J. Chem. Phys.* **2005**, *122*, 14.
(8) Zawodzinski, T. A., Jr.; Derouin, C.; Radzinski, S.; Sherman, R. J.; Smith, V. T.; Springer, T. E.; Gottesfeld, S. *J. Electrochem. Soc.* **1993**, *140*, 1041.
(9) Becke, A. D. *J. Chem. Phys.* **1993**, *98*, 5648.
(10) Frisch, M. J.; Pople, J. A.; Binkley, J. S. *J. Chem. Phys.* **1984**, *80*, 3265.
(11) Clark, T.; Chandrasekhar, J.; Spitznagel, G. W.; Schleyer, P. V. R. *J. Comput. Chem.* **1983**, *4*, 294.
(12) Langlois, J. M.; Muller, P. R.; Coley, T. R.; Goddard, W. A.; Ringnalda, M. N.; Won, Y. F. R. *J. Chem. Phys.* **1990**, *92*, 7488.
(13) Paddison, S. J. *J. New Mater. Electrochem. Syst.* **2001**, *4*, 197.
(14) Spitznagel, G.; Timothy, C.; Paul von Ragué, S.; Warren, J. H. *J. Comput. Chem.* **1987**, *8*, 1109.
(15) Glezakou, V. A.; Dupuis, M.; Mundy, C. J. *Phys. Chem. Chem. Phys.* **2007**, *9*, 5752–5760.
(16) Li, X. B.; Liao, S. J. *J. Mol. Struct.: THEOCHEM* **2009**, *897* (1−3), 66–68.
(17) Sagarik, K.; Phonyiem, M.; Lao-Ngam, C.; Chaiwongwattana, S. *Phys. Chem. Chem. Phys.* **2008**, *10*, 2098–2112.
(18) Koyama, M.; Bada, K.; Sasaki, K.; Tsuboi, H.; Endou, A.; Kubo, M.; Del Carpio, C. A.; Broclawik, E.; Miyamoto, A. *J. Phys. Chem. B* **2006**, *110*, 17872–17877.
(19) Okamoto, Y. *Chem. Phys. Lett.* **2004**, *389*, 64.
(20) This calculated value corresponds to the experimental 969 cm^{-1}, not to be confused with the experimental 983 cm^{-1} .